ESAIM: M2AN 50 (2016) 1585–1613
DOI: 10.1051/m2an/2015094

ESAIM: Mathematical Modelling and Numerical Analysis
www.esaim-m2an.org

ENERGY CONSERVATIVE FINITE ELEMENT SEMI-DISCRETIZATION FOR VIBRO-IMPACTS OF PLATES ON RIGID OBSTACLES

Cédric Pozzolini[1], Yves Renard[1] and Michel Salaün[2]

Abstract. Our purpose is to describe and compare some families of fully discretized approximations and their properties, in the case of vibro-impact of plates between rigid obstacles with non-penetration Signorini's conditions. To this aim, the dynamical Kirchhoff–Love plate model is considered and an extension to plates of the singular dynamic method, introduced by Renard and previously adapted to beams by Pozzolini and Salaün, is described. A particular emphasis is given in the use of an adapted Newmark scheme in which intervene a discrete restitution coefficient. Finally, various numerical results are presented and energy conservation capabilities of several numerical schemes are investigated and discussed.

Mathematics Subject Classification. 35L85, 65M12, 74H15, 74H45.

Received March 9, 2015. Revised September 18, 2015. Accepted December 1st, 2015.

1. Introduction

The obtention of reliable and predictive simulations of the dynamics with impacts of thin plates with existing numerical schemes remains very difficult. The vibro-impact of thin structures, plates and beams, intervene in the study of many complex industrial structures. For instance, it is the case of structures which originally motivated this study, namely satellite solar arrays. Indeed, during the launch of a satellite, the level of excitation is very high and the repeated impacts introduce strong nonlinearities which give the interpretation of measured signals very difficult.

Vibro-impact has been the subject of a wide literature which is particularly developped for rigid multi-body dynamics (see for instance [4, 17, 22]). A main difficulty for modeling impacts of thin structures is that, for usual models (Kirchhoff–Love or Mindlin–Reissner), the elasticity along the thickness is not taken into account. Accordingly, at impact, the plate should instantly rebound and the level of restitution during impact must be modeled. Contrary to what has been studied for the impact of rigid bodies, the relationship between numerical schemes and impact law has not been established for thin elastic structures. Even the expression of such a restitution law for thin elastic structures remains an open question.

Keywords and phrases. Variational inequalities, finite element method, elastic plates, dynamics, unilateral constraints.

[1] Université de Lyon, CNRS, INSA-Lyon, ICJ UMR5208, LaMCoS UMR5259, 69621 Villeurbanne, France.
cedric.pozzolini@insa.fr;yves.renard@insa-lyon.fr

[2] Université de Toulouse, CNRS, ISAE-SUPAERO, Institut Clément Ader (ICA), 31077 Toulouse cedex 4, France.
michel.salaun@isae.fr

Article published by EDP Sciences

Nevertheless, an important result in that domain is due to Dumont and Paoli [10] and deals with vibro-impact of Euler–Bernouilli beams. They show the weak convergence of a subsequence of numerical solutions, obtained with finite elements in space and a (β, γ)-Newmark scheme (for $\gamma = 1/2$) in time. Moreover, a conditional stability for $\beta \in [0, 1/2)$ is established together with an inconditional stability for $\beta = 1/2$. However, no information on any restitution law at impact is exhibited for the limit solution. Then, in [28], we have extended Dumont's and Paoli's results to Kirchhoff–Love plates for $\beta = \gamma = 1/2$. So we have presented a convergence result of a fully discrete scheme toward one solution of the continuous problem. This established both an existence result for the solution of the continuous problem and ensured that one subsequence weakly converged toward this solution. But we have not obtained any uniqueness result. In particular, such a result would certainly require the ability to express an additional impact law (see [22, 24]). Moreover, in [28], we have also presented some numerical experiments, using a classical Newmark scheme, which means use of a "classical" mass matrix (in opposition to the reduced mass matrix which will be introduced in the following), and which is fully implicit (that will be interpreted further as an absorbing shock). Those numerical results exhibited a decrease of mechanical energy of the plate, due to impacts, while it should have been conserved in the case of a perfect impact. This case will also be studied in Section 4.4. Following [27], in which an Euler–Bernouilli beam model was studied, this paper aims at addressing the problems of energy conservation and impact law in numerical schemes for bending plates.

Another difficulty appears in elastodynamic contact problems. Most of usual numerical schemes exhibit spurious oscillations on the contact displacement and stress (see for instance [18]). This has already led to many researches and a great variety of solutions were proposed. A first idea is to add damping terms, but it leads to a loss of accuracy on the solution. However, let us remark that adding damping leads to some existence results, such as [19]. Another way is to implicit the contact stress (see [5,9]) but kinetic energy of the contacting nodes is lost at each impact. Looking for some energy conserving schemes is now a widely adressed problem, see for example [15, 20, 21, 30]. Nevertheless, the proposed schemes exhibit large oscillations on the contact stress. Besides, most of them do not strictly respect the constraint. Moreover, the way to establish balance of energy is a mathematicaly very difficult problem, even in the simple case of viscoelastic bar model with Signorini condition (see [25, 26]).

In [18], the authors studied the numerical instabilities caused by spatial semi-discretization for linear elastodynamics frictionless contact problems in the small deformations framework. It was shown that the main cause of ill-posedness is due to the inertia of the nodes on the contact boundary. Then an original Mass Redistribution Method (MRM) which consists in the redistribution of the mass near the contact boundary is proposed to recover the well-posedness of the semi-discrete problem and ensures the solution to be energy conserving for elastic frictionless contact problems. Furthermore the MRM eliminates spurious oscillations on the contact boundary and respects the non-penetration constraint. Following the seminal work of [18], the authors of [8, 12, 14, 16] exploit the mass reduction technique to treat other dynamic contact problems.

An insight to the ill-posedness origin was given by Renard [29] as an adapted modified mass method (inspired from the MRM, and named "singular dynamic method"). Indeed, it is known that velocities may be discontinuous when an impact occurs. But velocities are regularized by a classical finite element discretization of the displacement, with concentration of the mass to the nodes. The singular dynamic method consists in performing different space semi-discretization for the velocity and displacement. Then the mass term is modified (in such a way that the mass matrix is singular) and the contact condition is enforced by a variable inequality. Owing to this mass modification, inertial forces cannot trigger spurious oscillations at the boundary. Furthermore, the system tends to conserve its energy in frictionless contact problem, which ensures a good behavior in long time.

As the Kirchhoff–Love plate model is obtained by the same kind of assumptions than the Euler–Bernoulli beam theory for bending, it is natural to expect to improve vibro-impacts numerical simulations by the same way. Then, in this study, we use the singular dynamic method introduced in [29] and we follow the ideas introduced in [27], for Euler–Bernouilli beam model, to extend those works to the Kirchhoff–Love plate model. So it can be hoped this method will provide energy conserving finite element semi-discretizations.

So, this paper is organized as follows. In the next section, the model problem we adress is described. Then, the so-called singular dynamic method is introduced, for which stable singular mass matrices schemes are derived in the case of our plate model. In Section 4 and 5, two fully discretized schemes are presented: a first one derived from the Newmark scheme, with an adaptation that is intended to model a restitution coefficient, and a second one obtained with a midpoint rule. Various numerical results investigate energy conservation capabilities of the previous schemes.

2. Notations and statement of the problem

2.1. Variational formulation of the plate model

Let us consider a thin elastic plate *i.e.* a plane structure for which one dimension, called the thickness, is very small compared to the others. For this kind of structures, starting from *a priori* hypotheses on the expression of the displacement fields, a two-dimensional problem is usually derived from the three-dimensional elasticity formulation by means of integration along the thickness. Then, the unknown variables are set down on the mid-plane of the plate.

Let Ω be an open, bounded, connected subset of the plane $\mathbb{R}^2$, with Lipschitz boundary. It will define the mid-plane of the plate. Then, the plate in its stress free reference configuration coincides with domain

$$\Omega^\varepsilon = \Omega \times \,]-\varepsilon\ ,\ +\varepsilon[= \left\{\ (x_1,x_2,x_3) \in \mathbb{R}^3\ /\ (x_1,x_2) \in \Omega \text{ and } x_3 \in\,]-\varepsilon\ ;\ \varepsilon[\ \right\},$$

where $2\ \varepsilon > 0$ is called the thickness.

In plate theory, it is usual to consider the following approximation of the three-dimensional displacements for $(x_1,x_2,x_3)\ \in\ \Omega^\varepsilon$

$$\left\{\begin{array}{l} u_1(x_1,x_2,x_3) = \overline{u}_1(x_1,x_2) + x_3\ \psi_1(x_1,x_2) \\ u_2(x_1,x_2,x_3) = \overline{u}_2(x_1,x_2) + x_3\ \psi_2(x_1,x_2) \\ u_3(x_1,x_2,x_3) = u_3(x_1,x_2). \end{array}\right. \tag{2.1}$$

In these expressions, $\overline{u}_1$ and $\overline{u}_2$ are the membrane displacements of the mid-plane points, u_3 is the deflection, while ψ_1 and ψ_2 are the section rotations. In the case of an homogeneous isotropic material, the variational plate model splits into two independent problems: the first, called the membrane problem, deals only with membrane displacements, while the second, called the bending problem, concerns deflection and rotations. In this paper, only the bending problem is addressed, and we shall consider the Kirchhoff–Love model, which can be seen as a particular case of (2.1) obtained by introducing the so-called Kirchhoff–Love assumptions

$$\psi = -\nabla\ u_3 \quad \Leftrightarrow \quad \left\{\begin{array}{l} \psi_1 = -\partial_1\ u_3, \\ \psi_2 = -\partial_2\ u_3, \end{array}\right.$$

where ∂_α stands for the partial derivative with respect to x_α , for $\alpha = 1$ or 2. Consequently, the deflection is the only unknown for the bending Kirchhoff–Love plate problem. For convenience, it will be denoted by u all along the following of this paper. So, if f is the resulting transverse loading, the variational formulation of the Kirchhoff–Love elastodynamical model for a thin elastic plate reads as

$$\left\{\begin{array}{l} \text{Find } u = u(x,t) \text{ with } (x,t)\ \in\ \Omega\ \times\ [0,T] \text{ such that for any } w \in \mathbb{V} \\ \displaystyle\int_\Omega 2\rho\varepsilon\ \frac{\partial^2 u}{\partial t^2}\ w\ \mathrm{d}x + \int_\Omega \frac{2\ E\ \varepsilon^3}{3\ (1-\nu^2)}\ \left[(1-\nu)\ \partial^2_{\alpha\beta}u + \nu\ \Delta u\ \delta_{\alpha\beta}\right]\ \partial^2_{\alpha\beta}w\ \mathrm{d}x = \int_\Omega f\ w\ \mathrm{d}x, \end{array}\right. \tag{2.2}$$

where $\partial^2_{\alpha\beta}u = \dfrac{\partial^2 u}{\partial x_\alpha\ \partial x_\beta}$. The associated initial conditions are

$$u(x,0) = u_0(x), \quad \frac{\partial u}{\partial t}(x,0) = v_0(x), \quad \forall x\ \in\ \Omega. \tag{2.3}$$

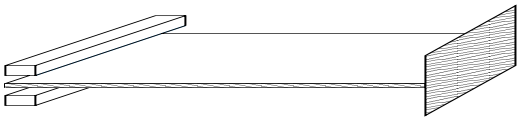

FIGURE 1. Example of bending clamped plate between rigid obstacles.

In (2.2), the mechanical constants, for a plate made of a homogeneous and isotropic material, are its Young's modulus E, its Poisson's ratio ν and its mass density ρ. Moreover, $\delta_{\alpha\beta}$ is the Kronecker's symbol and the summation convention over repeated indices is adopted, Greek indices varying in $\{1,2\}$. If the plate is assumed to be clamped on a non-zero Lebesgue measure part of the boundary $\partial\Omega$ denoted Γ_c and free on Γ_f , such as $\partial\Omega = \Gamma_c \cup \Gamma_f$, the space of admissible displacements is

$$\mathbb{V} = \{\ w \in H^2(\Omega)\ /\ w(x) = 0 = \partial_n w(x)\ ,\ \forall x\ \in\ \Gamma_c\ \}, \tag{2.4}$$

where $\partial_n w$ is the normal derivative along Γ_c and $H^2(\Omega)$ is the classical Sobolev space, the definition of which can be found in [1] for instance. Finally, let us recall that (2.2) is well-posed, as the bilinear form $a\ :\ \mathbb{V}\times\mathbb{V}\ \to\ \mathbb{R}$ defined by

$$a(u,w) = \int_\Omega \frac{2\ E\ \varepsilon^3}{3\ (1-\nu^2)}\ \left[(1-\nu)\ \partial^2_{\alpha\beta}u + \nu\ \Delta u\ \delta_{\alpha\beta}\right]\ \partial^2_{\alpha\beta}w\ \mathrm{d}x, \tag{2.5}$$

is a scalar product on $\mathbb{V}$ which is equivalent to the canonical scalar product of $H^2(\Omega)$ (for more details, see [28] for example).

2.2. Vibro-impact formulation of the plate model

Let us now introduce the dynamic frictionless Kirchhoff–Love equation with Signorini's contact conditions along the plate. We assume that the plate motion is limited by rigid obstacles, located above and below the plate (see Fig. 1). So, the displacement is constrained to belong to the convex set $\mathbb{K}\ \subset\ \mathbb{V}$ given by

$$\mathbb{K} = \{w \in \mathbb{V}\ /\ g_1(x)\ \le\ w(x)\ \le\ g_2(x),\quad \forall x \in \Omega\}, \tag{2.6}$$

where g_1 and g_2 are two mappings from Ω to $\bar{\mathbb{R}} := \mathbb{R}\cup\{-\infty,+\infty\}$ such that there exists $g\ >\ 0$ with

$$g_1(x)\ \le\ -g\ <\ 0\ <\ g\ \le\ g_2(x),\quad \forall x \in \Omega. \tag{2.7}$$

Then, the mechanical frictionless elastodynamic problem for a plate between two rigid obstacles can be written as the following variational inequality

$$\begin{cases} \text{Find } u\ :\ [0,T]\to\mathbb{K} \text{ such that for almost every } t\in[0,T] \text{ and for every } w\in\mathbb{K} \\ \displaystyle\int_\Omega 2\rho\varepsilon\ \frac{\partial^2 u}{\partial t^2}(t)\ (w-u(t))\ \mathrm{d}x + a(u(t),w-u(t))\ \ge\ \int_\Omega f\ (w-u(t))\ \mathrm{d}x \\ \displaystyle u(x,0) = u_0(x) \in \mathbb{K},\quad \frac{\partial u}{\partial t}(x,0) = v_0(x)\quad \forall x\in\Omega. \end{cases} \tag{2.8}$$

Setting $\mathbb{H} = L^2(\Omega)$, if it is assumed that $f \in L^2(0,T;\mathbb{H})$, $u_0 \in \mathbb{K}$ and $v_0 \in \mathbb{H}$, we proved in [28] that problem (2.8) has a solution u belonging to $L^2(0,T;\mathbb{K})$. For this, we have extended to plates a result for Euler–Bernouilli beams due to Dumont and Paoli [10], who established convergence of the solutions of fully discretized approximations of the problem. As far as uniqueness is concerned, as a counterexample has been given in [2] for beams, we cannot expect it for (2.8). Finally, there is no result about conservation of energy at the limit.

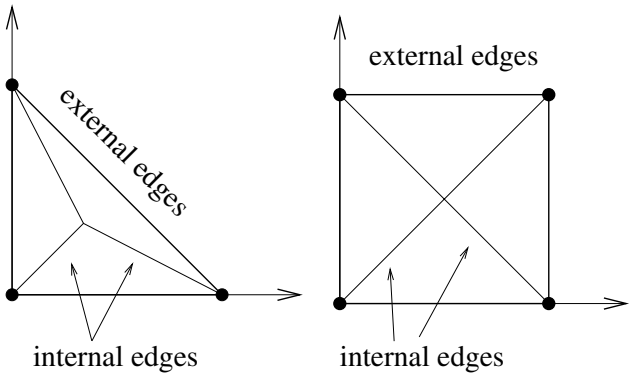

FIGURE 2. HCT triangle and FVS quadrangle. Location of degrees of freedom and sub-triangles.

In fact, problem (2.8) does not describe completely the motion. A constitutive law for impact should be added (see [22]). For example, if there is an impact at point x_0 and time t_0, this law should give the relation between velocities before and after impact

$$\frac{\partial u}{\partial t}(x_0, t_0^+) = -e\ \frac{\partial u}{\partial t}(x_0, t_0^-), \tag{2.9}$$

where scalar e, called restitution coefficient, is a real number belonging to $[0, 1]$. $e = 1$ matches to a perfect impact: Velocity is conserved, up to its sign, whereas $e = 0$ is an absorbing shock. Let us remark that, in [24], the authors show that the restitution coefficient for a bar is a rather ill-defined concept. For instance, their numerical experiments underline the observed restitution coefficient depends very strongly on the initial angle of the bar with horizontal. Moreover, in the particular case of a slender bar dropped on a rigid foundation, the chosen value of the restitution coefficient does not seem to have a great influence on the displacement limit when the space step tends to zero. Despite the previous remarks, our idea is to explicitly incorporate those restitution coefficient into (2.8), particularly when $e = 1$, and to observe how some numerical schemes will simulate the experimental behavior of a vibrating plate.

3. Singular dynamic method

3.1. Finite element model for the plate problem

First, let us introduce the space discretization of the displacement. As the Kirchhoff–Love model corresponds to a fourth order partial differential equation, a finite dimensional approximation space $\mathbb{V}^h$ of the continuous space $H^2(\Omega)$ has to be built. In order to have a conformal method, *i.e.* $\mathbb{V}^h \subset H^2(\Omega)$, functions of $\mathbb{V}^h$ must be continuously differentiable, which needs the use of $\mathcal{C}^1$ finite elements. Among the available elements having this regularity (see [6]), the reduced HCT (Hsieh–Clough–Tocher) triangles and FVS (Fraeijs de Veubeke–Sanders) quadrangles are of particular interest. For the HCT (resp. FVS) element, the triangle (resp. quadrangle) is divided into three (resp. four) sub-triangles (see Fig. 2). The basis functions of these elements are P_3 polynomials on each sub-triangle and matched $\mathcal{C}^1$ across each internal edge. In addition, to decrease the number of degrees of freedom, the normal derivative is assumed to vary linearly along the external edges of the elements (this assumption does not hold on the internal edges). Finally, both for triangles and quadrangles, there are only three degrees of freedom on each node: The values of the function and its first derivatives. So, these elements have the two following properties:

(1) With the reduction, the computational cost is limited to three degrees of freedom for each node of the mesh, like a classical Mindlin–Reissner element for which each node has also three degrees of freedom (the deflection and the two section rotations).

(2) For regular problems (see [7]), the theoretical error is in $O(h)$ for the *energy norm* and $O(h^2)$ for the *displacement norm*, where h stands for the mesh parameter.

Then, the reduced HCT or FVS elements and the standard Mindlin elements have the same features as far as numerical cost and accuracy are concerned.

Remark 3.1. In the following numerical tests, we shall also consider the complete HCT triangle and the classical Argyris triangle, which uses P_5 polynomials and is another $\mathcal{C}^1$ finite element.

3.2. Well-posed space semi-discretization

The goal of this section is to present a well-posed space semi-discretization of problem (2.8). As usual, a Galerkin method is used for space discretization but the original idea, due to Renard [29], is to introduce different approximations for displacement u and velocity $v = \frac{\partial u}{\partial t}$. So, let $\mathbb{V}^h$ and $\mathbb{H}^h$ be two finite dimensional vector subspaces of $\mathbb{V}$ and $\mathbb{H}$ respectively. Let $\mathbb{K}^h \subset \mathbb{V}^h$ be a closed convex nonempty approximation of $\mathbb{K}$. The new approximation of (2.8) reads

$$\begin{cases} \text{Find } u^h : [0,T] \to \mathbb{K}^h \text{ and } v^h : [0,T] \to \mathbb{H}^h \text{ such that for all } t \in (0,T] \\ \displaystyle\int_\Omega 2\rho\varepsilon \, \frac{\partial v^h}{\partial t} \, (w^h - u^h) + a(u^h, w^h - u^h) \geq \int_\Omega f \, (w^h - u^h) \, \mathrm{d}x, \quad \forall \, w^h \in \mathbb{K}^h \\ \displaystyle\int_\Omega 2\rho\varepsilon \, \left(v^h - \frac{\partial u^h}{\partial t} \right) \, q^h \, \mathrm{d}x = 0, \quad \forall \, q^h \in \mathbb{H}^h \\ u^h(x,0) = u_0^h(x), \quad v^h(x,0) = v_0^h(x), \quad \forall x \in \Omega, \end{cases} \tag{3.1}$$

where $u_0^h \in \mathbb{K}^h$ and $v_0^h \in \mathbb{H}^h$ are approximations of u_0 and v_0 respectively. The case $\mathbb{H}^h = \mathbb{V}^h$ clearly corresponds to a standard Galerkin approximation of (2.8).

Let us now introduce some basis of $\mathbb{V}^h$ and $\mathbb{H}^h$, say respectively ϕ_i $(1 \leq i \leq N_V)$ and ψ_i $(1 \leq i \leq N_H)$. The above discrete variational formulation is associated with matrices $\mathbf{K}$ (stiffness matrix), $\mathbf{B}$ and $\mathbf{C}$ (mass matrices) of respective sizes N_V^2 , $N_H \times N_V$ and N_H^2 , defined by

$$\mathbf{K}_{ij} = a(\phi_i \, , \, \phi_j), \quad \mathbf{B}_{ij} = \int_\Omega 2\rho\varepsilon \, \psi_i \, \phi_j \, \mathrm{d}x, \quad \mathbf{C}_{ij} = \int_\Omega 2\rho\varepsilon \, \psi_i \, \psi_j \, \mathrm{d}x.$$

The related vectors, say F, U (components u_i) and V (components v_i), of size N_V , N_V and N_H respectively, are such that

$$F_i = \int_\Omega f \, \phi_i \, \mathrm{d}x, \quad u^h(t) = \sum_{i=1}^{N_V} u_i(t)\phi_i, \quad v^h(t) = \sum_{i=1}^{N_H} v_i(t)\psi_i.$$

Let us introduce the notations $\dot{W} = \dfrac{\partial W}{\partial t}$ and $\ddot{W} = \dfrac{\partial^2 W}{\partial t^2}$. We remark that the second equation of (3.1) reads

$$\mathbf{C} \, V(t) = \mathbf{B} \, \dot{U}(t).$$

Since $\mathbf{C}$ is always invertible, we obtain $V(t) = \mathbf{C}^{-1} \, \mathbf{B} \, \dot{U}(t)$ and, then, $\dot{V}(t) = \mathbf{C}^{-1} \, \mathbf{B} \, \ddot{U}(t)$, which allows to eliminate V. So the semi-discretized problem (3.1) is equivalent to

$$\begin{cases} \text{Find } U : [0,T] \to \mathbb{K}^h \text{ and } V : [0,T] \to \mathbb{H}^h \text{ such that for all } t \in (0,T] \\ (W - U(t))^T \, (\mathbf{M}\ddot{U}(t) + \mathbf{K}U(t)) \geq (W - U(t))^T \, F, \quad \forall W \in \mathbb{K}^h, \\ \mathbf{C} \, V(t) = \mathbf{B} \, \dot{U}(t), \\ U(0) = U_0, \quad V(0) = V_0, \end{cases} \tag{3.2}$$

where $\mathbf{M}$ is the so-called singular mass matrix defined by

$$\mathbf{M} = \mathbf{B}^T\ \mathbf{C}^{-1}\ \mathbf{B}. \tag{3.3}$$

Let us now explain how the approximation $\mathbb{K}^h$ of $\mathbb{K}$ is obtained. We recall that

$$\mathbb{K} = \{w \in \mathbb{V}\ /\ g_1(x)\ \leq\ w(x)\ \leq\ g_2(x),\quad \forall x \in \Omega\}.$$

For $1\ \leq\ i\ \leq\ N_N$, let x_i be the nodes of the mesh, except those which are clamped. Then, unilateral constraints are only considered at these nodes. It means convex $\mathbb{K}^h$ is

$$\mathbb{K}^h = \{w^h \in \mathbb{V}^h\ /\ g_1(x_i)\ \leq\ w^h(x_i)\ \leq\ g_2(x_i),\quad 1\ \leq\ i\ \leq\ N_N\}. \tag{3.4}$$

With vector notations, setting $\alpha_i^-\ \equiv\ g_1(x_i)$ and $\alpha_i^+\ \equiv\ g_2(x_i)$ for all i, this space may be written (we keep the same notation for simplicity)

$$\mathbb{K}^h = \{W \in \mathbb{R}^{N_V}\ /\ \alpha_i^-\ \leq\ (G^i)^T\ W \leq \alpha_i^+,\quad 1\ \leq\ i\ \leq\ N_N\},$$

where G^i is the vector of $\mathbb{R}^{N_V}$ such that $(G^i)^T\ W = w^h(x_i)$, for each node x_i .

Remark 3.2. As seen in Section 3.1, since we deal with a fourth order problem with respect to the space derivative, it is not possible to consider a linear space approximation. In fact, for this plate model, the degrees of freedom are node displacements and their derivatives. So, in the above approximation of $\mathbb{K}$, we consider only constraints on node displacements: In particular, the effect of the first derivatives, namely the curvature, is not taken into account. Then, in this framework, the plate could cross the obstacle between two nodes, but we shall neglect this aspect in the following.

Furthemore, functions g_1 and g_2 take their values in $\bar{\mathbb{R}}$, which means that $\alpha_i^{\pm}$ may be equal to $\pm\infty$. In this case, the corresponding constraint is worthless. For instance, it will be the case if the obstacles are reduced to end stops along one edge of the plate (see Fig. 1). Moreover, it is assumed that the clamped edge satisfies the constraints. So, it is natural to introduce the number, say N_G , of "real" constraints. For example, N_G is equal to N_N for flat obstacles up and under all the plate.

Now, let us introduce matrix $\mathbf{G}$, of size $N_G\ \times\ N_V$, which components are $\mathbf{G}_{ij} = (G^i)_j$. As the previous choice is clearly such that vectors G^i are linearly independent, using the Lagrange multipliers, the discrete problem (3.2) is also equivalent to the following one

$$\left\{\begin{array}{l}
\text{Find } U\ :\ [0,T] \to \mathbb{K}^h \text{ and } V\ :\ [0,T] \to \mathbb{H}^h \text{ such that for all } t \in (0,T] \\[2ex]
\mathbf{M}\ddot{U}(t) + \mathbf{K}U(t) = F + \displaystyle\sum_{i=1}^{N_G} \Lambda^i(t) G^i, \\[2ex]
\left\{\begin{array}{l}
\Lambda^i(t) \geq 0\ ,\ (G^i)^T\ U(t)\ \geq\ \alpha_i^-\ ,\ \Lambda^i(t)\ \left((G^i)^T\ U(t) - \alpha_i^-\right) = 0 \\
\text{or} \\
\Lambda^i(t) \leq 0\ ,\ (G^i)^T\ U(t)\ \leq\ \alpha_i^+\ ,\ \Lambda^i(t)\ \left((G^i)^T\ U(t) - \alpha_i^+\right) = 0
\end{array}\right\}\quad 1 \leq i \leq N_G, \\[2ex]
\mathbf{C}\ V(t) = \mathbf{B}\ \dot{U}(t), \\[2ex]
U(0) = U_0,\quad V(0) = V_0.
\end{array}\right. \tag{3.5}$$

Here, the Lagrange multipliers Λ^i are the reaction forces.

Now, let us introduce the following subspace $\mathbb{F}^h$ of $\mathbb{V}^h$, defined by

$$\mathbb{F}^h = \left\{w^h \in \mathbb{V}^h\ /\ \int_\Omega 2\rho\varepsilon\ w^h\ \xi^h \mathrm{d}x = 0,\quad \forall \xi^h \in \mathbb{H}^h\right\}.$$

With the previous definitions, we have: $\mathbb{F}^h = \ker \mathbf{B}$, and the proof of the following result is given in [29].

Theorem 3.3. *If $\mathbb{V}^h$, $\mathbb{H}^h$ and $\mathbb{K}^h$ satisfy the following Inf-Sup condition*

$$\inf_{Q\in\mathbb{R}^{N_G}\setminus\{0\}} \sup_{W\in\mathbb{F}^h\setminus\{0\}} \frac{Q^T\ \mathbf{G}\ W}{\|Q\|\ \|W\|} \ >\ 0, \tag{3.6}$$

then problem (3.2) has a unique solution $U(t)$. Moreover, this solution is Lipschitz-continuous with respect to t and verifies the following persistency condition

$$\Lambda^i(t)\ (G^i)^T\ \dot{U}(t) = 0, \quad \forall t \in (0,T], \quad 1 \le i \le N_G.$$

Finally, solution $U(t)$ is energy conserving in the sense that the discrete energy

$$E^h(t) = \frac{1}{2}\ \dot{U}^T(t)\ \mathbf{M}\ \dot{U}(t) + \frac{1}{2}\ U^T(t)\ \mathbf{K}\ U(t)\ -\ U^T(t)\ F,$$

is constant with respect to t.

Remark 3.4. The persistency condition (see [20, 21]), which links velocity $\dot{U}(t)$ and reaction forces Λ^i, is a stronger condition than the classical complementary condition between solution $U(t)$ and Lagrange multipliers Λ^i. It is important to note that energy conservation is proved thanks to those persistency condition.

3.3. Numerical discretization

Thanks to the above theorem, proving condition (3.6) is sufficient to obtain well-posedness of the discrete problem (3.2). Let us remark this condition is equivalent to the fact that matrix $\mathbf{G}$ is surjective on $\mathbb{F}^h$. So we must have

$$\dim \mathbb{F}^h\ \ge\ N_G \qquad \text{and then} \qquad \dim \mathbb{H}^h\ \le\ \dim \mathbb{V}^h\ -\ N_G.$$

This prescribes conditions on the approximation spaces $\mathbb{V}^h$, $\mathbb{H}^h$ and also $\mathbb{K}^h$. In practice, for our space discretizations, the following finite element schemes are chosen (see Sect. 3.1):

- For triangles: Velocity is constant on each element (P_0 approximation) while displacement uses complete HCT, reduced HCT or Argyris elements.
- For quadrangles: Velocity is constant again on each element (Q_0 approximation) while displacement uses reduced FVS elements.

So, here, the dimension of $\mathbb{H}^h$, say N_H, is equal to the number of elements of the mesh.

For Euler–Bernouilli beam model and Hermite's finite elements, inf-sup condition (3.6) has been established theoretically in [27]. In the case of our plate model and our finite element method, a direct proof of such an inf-sup condition is a more difficult question and remains open. Nevertheless, we suggest a numerical verification. It is given by the following lemma which presents a sufficient condition to ensure (3.6).

Lemma 3.5. *If one subdivises the set of degrees of freedom into two groups:*

- *The first group contains the degrees of freedom which intervene in vectors G^i , $1 \le i \le N_G$, representing the contact conditions (in our case, the degrees of freedom representing the transverse displacement),*
- *The second group contains the remaining degrees of freedom (in our case, the derivative ones).*

If vectors G^i are linearly independent and if the sub-matrix of $\mathbf{B}$, being the restriction of $\mathbf{B}$ to the columns corresponding to the degrees of freedom of the second group, is of rank N_H (which is the number of rows of $\mathbf{B}$), then we can conclude that the inf-sup condition (3.6) is satisfied.

Proof. If the hypotheses are satisfied, then for each vector G^i corresponding to a contact condition, the linear combination of column of $\mathbf{B}$ corresponding to the product $\mathbf{B}G^i$ can be written has a linear combination of the column of $\mathbf{B}$ corresponding to the degrees of freedom of the second group. Consequently, for each vector G^i,

we can build a vector $Z_i \in \mathbb{F}^h$ which is equal to G^i on the components corresponding to the degrees of freedom of the first group. Since vectors G^i are linearly independent, vectors Z_i are also independent and the square matrix $\bar{G}$ being the restriction of G to the subspace spanned by Z_i , $1 \leq i \leq N_G$, is invertible. This is sufficient to satisfy (3.6) since it means that, for any vector $Q \in \mathbb{R}^{N_G}$, there exists a linear combination $\bar{Z}$ of Z_i such that $Q = \mathbf{G}\bar{Z}$ and $\mathbf{G}$ is surjective on $\mathbb{F}^h$. □

In our case, the vectors G^i are linearly independent. Thus it is sufficient to check numerically that there exists a subset of columns of $\mathbf{B}$, associated with the derivative degrees of freedom, which contains a family of linearly independant vectors, which size is equal to the number of elements of the mesh. In all the forthcoming numerical tests, this condition was numerically checked.

4. Fully discretized Newmark-type schemes

In this section, we introduce and test β-Newmark schemes for time discretization, in the cases of regular and singular mass matrices. These schemes are interesting since they are energy conserving during the linear part of the motion (equation without constraint). The goal of this section is then to study their capabilities to be energy conserving in the non-linear case. In addition, Δt will be the time step and e the restitution coefficient.

4.1. Case of a regular mass matrix

As Dumont–Paoli [10] for beams and us [28] for plates, to solve problem (2.8), the following implicit $(\beta, \gamma = 1/2)$-Newmark scheme is used

$$\left\{\begin{array}{l} \text{Find } U^{n+1} \in \mathbb{K}^h \text{ such that for all } W \in \mathbb{K}^h \\ \\ \left(W - U^{n+1}\right)^T \left(\mathbf{M}_r \, \dfrac{U^{n+1} - 2U^n + U^{n-1}}{\Delta t^2} + \mathbf{K} \, \left(\beta U^{n+1} + (1-2\beta)U^n + \beta U^{n-1}\right)\right) \\ \\ \qquad \geq \left(W - U^{n+1}\right)^T \, F^{n,\beta} \end{array}\right. \tag{4.1}$$

where

$$F^{n,\beta} = \beta F^{n+1} + (1-2\beta)F^n + \beta F^{n-1}, \tag{4.2}$$

F^k being the vector which components are $F_i^k = \displaystyle\int_\Omega f(x, k\Delta t) \; \phi_i(x) \; \mathrm{d}x$. Finally, $(\phi_i)_i$ stand for the basis functions defining space $\mathbb{V}^h$ and $\mathbf{M}_r$ is the associated regular mass matrix, which generic term reads

$$(\mathbf{M}_r)_{ij} = \int_\Omega 2\rho\varepsilon \; \phi_i \; \phi_j \; \mathrm{d}x.$$

To take into account the restitution coefficient e defined by (2.9), we follow Paoli–Schatzman (see [23, 24]). It consists in replacing U^{n+1} by $\frac{U^{n+1} + e \; U^{n-1}}{1+e}$. Then, a more general discretization of (2.8) becomes the e-β-Newmark scheme

$$\left\{\begin{array}{l} \text{Find } U^{n+1,e} \;\equiv\; \dfrac{U^{n+1} + eU^{n-1}}{1+e} \in \mathbb{K}^h \text{ such that for all } W \in \mathbb{K}^h \\ \\ (W - U^{n+1,e})^T \left(\mathbf{M}_r \, \dfrac{U^{n+1} - 2U^n + U^{n-1}}{\Delta t^2} + \mathbf{K} \, \left(\beta U^{n+1} + (1-2\beta)U^n + \beta U^{n-1}\right)\right) \\ \\ \qquad \geq \left(W - U^{n+1,e}\right)^T \, F^{n,\beta}. \end{array}\right. \tag{4.3}$$

Let us remark that $(\beta, \gamma = 1/2)$-Newmark implicit scheme corresponds to $e = 0$. In this case, we established in [28] unconditional stability for $\beta = 1/2$ and a weak convergence result (up to a subsequence).

Remark 4.1. Let us define the total energy by

$$E(w,\dot{w}) \;:=\; \frac{1}{2}\int_\Omega 2\rho\varepsilon\ \dot{w}(x,t))^2\ \mathrm{d}x + \frac{1}{2}\,a(w(.,t)\ ,\ w(.,t)) \;-\; \int_\Omega f(x,t)\ w(x,t)\ \mathrm{d}x.$$

In general, for fully-discretized schemes, energy dissipation (i.e. $E(u^{n+1}\ ,\ v^{n+1}) \;\leq\; E(u^n\ ,\ v^n), \forall n$) can fail to hold. We would like to obtain a numerical scheme which energy is conserved as long as the plate does not touch the obstacles and which doesn't create energy when plate reaches them. The following numerical results will suggest that conservation of energy may hold for generic initial conditions, if a singular mass matrix is used.

4.2. Case of a singular mass matrix

To derive a Newmark scheme using the singular mass matrix approach, let us start from the equilibrium equation given in (3.5)

$$\mathbf{M}\,\ddot{U} + \mathbf{K}\,U = F + \Lambda \;\equiv\; \tilde{F},$$

where Λ stands for the reaction, which is zero when there is no contact. Moreover, the singular mass approach introduces matrices $\mathbf{C}$ and $\mathbf{B}$ such that $\mathbf{C}\,V = \mathbf{B}\,\dot{U}$, the singular mass matrix being $\mathbf{M} = \mathbf{B}^T\ \mathbf{C}^{-1}\ \mathbf{B}$. The usual $(\beta, 1/2)$-Newmark scheme reads

$$\begin{cases} U^{n+1} = U^n + \Delta t\ \dot{U}^n + (\frac{1}{2} - \beta)\ \Delta t^2 \ddot{U}^n + \beta \Delta t^2 \ddot{U}^{n+1}, \\ \dot{U}^{n+1} = \dot{U}^n + \frac{\Delta t}{2}\ddot{U}^n + \frac{\Delta t}{2}\ddot{U}^{n+1}. \end{cases}$$

Multiplying left by $\mathbf{B}$ and using $\mathbf{C}\,V = \mathbf{B}\,\dot{U}$, we deduce

$$\begin{cases} \mathbf{B}\,U^{n+1} = \mathbf{B}\,U^n + \Delta t\ \mathbf{C}\,V^n + (\frac{1}{2} - \beta)\ \Delta t^2 \mathbf{B}\,\ddot{U}^n + \beta \Delta t^2 \mathbf{B}\,\ddot{U}^{n+1}, \\ \mathbf{C}\,V^{n+1} = \mathbf{C}\,V^n + \frac{\Delta t}{2}\mathbf{B}\,\ddot{U}^n + \frac{\Delta t}{2}\mathbf{B}\,\ddot{U}^{n+1}. \end{cases} \tag{4.4}$$

It is well-known it is possible to derive a two-step scheme by eliminating velocity from this relations. First, we write

$$\begin{cases} \mathbf{B}\,U^n \;\;\;\;\;\;= \mathbf{B}\,U^{n-1} + \Delta t\ \mathbf{C}\,V^{n-1} + (\frac{1}{2} - \beta)\ \Delta t^2 \mathbf{B}\,\ddot{U}^{n-1} + \beta \Delta t^2 \mathbf{B}\,\ddot{U}^n, \\ \mathbf{B}\,U^{n+1} = \mathbf{B}\,U^n + \Delta t\ \mathbf{C}\,V^n + (\frac{1}{2} - \beta)\ \Delta t^2 \mathbf{B}\,\ddot{U}^n + \beta \Delta t^2 \mathbf{B}\,\ddot{U}^{n+1}, \end{cases}$$

which leads to

$$\begin{aligned} \mathbf{B}\,(U^{n+1} - 2\,U^n + U^{n-1}) = \Delta t\ \mathbf{C}\,(V^n \;-\; V^{n-1}) \\ + \Delta t^2\ \mathbf{B}\ \left(\beta \ddot{U}^{n+1} + \left(\frac{1}{2} - 2\beta\right)\ddot{U}^n - \left(\frac{1}{2} - \beta\right)\ddot{U}^{n-1}\right), \end{aligned}$$

and finally, with the second equation of (4.4), written at step n instead of $n+1$

$$\mathbf{B}\,(U^{n+1} \;-\; 2\,U^n + U^{n-1}) = \Delta t^2\ \mathbf{B}\ \left(\beta \ddot{U}^{n+1} + (1-2\beta)\ddot{U}^n + \beta \ddot{U}^{n-1}\right).$$

Multiplying this relation by $\mathbf{B}^T\ \mathbf{C}^{-1}$, we obtain

$$\mathbf{M}\,(U^{n+1} \;-\; 2\,U^n + U^{n-1}) = \Delta t^2\ \mathbf{M}\ \left(\beta \ddot{U}^{n+1} + (1-2\beta)\ddot{U}^n + \beta \ddot{U}^{n-1}\right),$$

where $\mathbf{M}$ is the singular mass matrix. As usual for Newmark scheme, we replace acceleration by its value, given by the equilibrium equation. Hence, in the case of the singular mass matrix approach, Newmark scheme reads

$$\begin{aligned} \mathbf{M}\,\frac{U^{n+1} \;-\; 2\,U^n + U^{n-1}}{\Delta t^2} + \mathbf{K}\left(\beta U^{n+1} + (1-2\beta)U^n + \beta U^{n-1}\right) \\ = \left(\beta \tilde{F}^{n+1} + (1-2\beta)\tilde{F}^n + \beta \tilde{F}^{n-1}\right), \end{aligned}$$

which looks exactly as the Newmark scheme except the regular mass matrix $\mathbf{M}_r$ has been replaced by the singular one. Therefore, in the case of Newmark scheme, the singular mass matrix approach leads to a scheme similar to (4.3)

$$\left\{\begin{array}{l} \text{Find } U^{n+1,e} = \dfrac{U^{n+1} + eU^{n-1}}{1+e} \in \mathbb{K}^h \text{ such that for all } W \in \mathbb{K}^h \\ \\ \left(W - U^{n+1,e}\right)^T \left(\mathbf{M}\, \dfrac{U^{n+1} - 2U^n + U^{n-1}}{\Delta t^2} + \mathbf{K}\, \left(\beta U^{n+1} + (1-2\beta)U^n + \beta U^{n-1}\right)\right) \\ \\ \qquad\qquad \geq \left(W - U^{n+1,e}\right)^T F^{n,\beta}. \end{array}\right. \tag{4.5}$$

To conclude, let us remark that, as matrix $\mathbf{K}$ is positive definite, this variational inequality has always a unique solution even if $\mathbf{M}$ is singular.

4.3. Some aspects of numerical implementation

To explain how the algorithm works in the general case, let us begin with the implicit ($e = 0$)-β-Newmark scheme (4.1). First, it can be rewritten as

$$\left\{\begin{array}{l} \text{Find } U^{n+1} \in \mathbb{K}^h \text{ such that for all } W \in \mathbb{K}^h \\ \\ \left(W - U^{n+1}\right)^T \left(\dfrac{\mathbf{M}_r}{\Delta t^2}\, U^{n+1} + \beta\, \mathbf{K} U^{n+1}\right) \geq \left(W - U^{n+1}\right)^T \tilde{F}^n \end{array}\right. \tag{4.6}$$

where

$$\tilde{F}^n = F^{n,\beta} - \mathbf{M}_r\, \frac{-2U^n + U^{n-1}}{\Delta t^2} - \mathbf{K}\, \left((1-2\beta)U^n + \beta U^{n-1}\right),$$

$F^{n,\beta}$ being given by (4.2). Since matrix $\mathbf{A} \equiv \frac{1}{\Delta t^2}\, \mathbf{M}_r + \beta\, \mathbf{K}$ is positive definite and symmetric, equation (5.4) is equivalent to the following minimization problem

$$U^{n+1} = \text{Argmin}_{W \in \mathbb{K}^h} \left(\frac{1}{2}\, W^T\, \mathbf{A}\, W - (\tilde{F}^n)^T\, W\right).$$

Let us remark that, as constraints defining $\mathbb{K}^h$ are linear, the above minimization problem is a linear quadratic problem, which is solved in Getfem++ [13] by an algorithm derived from the Alart–Curnier augmented Lagrangian formulation [3].

Now, as we look for energy conservative schemes, we consider also equation (4.3) but it is studied in the particular case $e = 1$, corresponding to a perfect impact. Then it reads

$$\left\{\begin{array}{l} \text{Find } \widetilde{U}^{n+1} = \dfrac{U^{n+1} + U^{n-1}}{2} \in \mathbb{K}^h \text{ such that for all } W \in \mathbb{K}^h \\ \\ (W - \widetilde{U}^{n+1})^T \left(\mathbf{M}_r\, \dfrac{U^{n+1} - 2U^n + U^{n-1}}{\Delta t^2} + \mathbf{K}\, \left(\beta U^{n+1} + (1-2\beta)U^n + \beta U^{n-1}\right)\right) \\ \\ \qquad\qquad \geq \left(W - \widetilde{U}^{n+1}\right)^T F^{n,\beta}. \end{array}\right.$$

Then, it is possible to express U^{n+1} as $U^{n+1} = 2\, \widetilde{U}^{n+1} - U^{n-1}$ and to replace it in the previous inequality

$$(W - \widetilde{U}^{n+1})^T \left(\mathbf{M}_r\, \frac{2\widetilde{U}^{n+1} - 2U^n}{\Delta t^2} + \mathbf{K}\, \left(2\beta\, \widetilde{U}^{n+1} + (1-2\beta)U^n\right)\right) \geq \left(W - \widetilde{U}^{n+1}\right)^T F^{n,\beta}$$

and the problem becomes

$$\begin{cases} \text{Find } \widetilde{U}^{n+1} \in \mathbb{K}^h \text{ such that for all } W \in \mathbb{K}^h \\ \left(W - \widetilde{U}^{n+1}\right)^T \left(\dfrac{\mathbf{M}_r}{\Delta t^2}\, \widetilde{U}^{n+1} + \beta\, \mathbf{K}\widetilde{U}^{n+1}\right) \geq \left(W - \widetilde{U}^{n+1}\right)^T G^n \end{cases} \tag{4.7}$$

where

$$G^n = \frac{1}{2}\left(F^{n,\beta} + \frac{2\,\mathbf{M}_r}{\Delta t^2}\, U^n - (1-2\beta)\,\mathbf{K}\, U^n\right).$$

It exactly looks like (5.4) and is solved in the same way.

Consequently, the way to solve (4.3) follows Paoli–Schatzman [24]. First, we calculate $Q^{n+1} \equiv \mathbf{A}^{-1}\, \tilde{F}^n$. Second, the following alternative holds:

- If $\dfrac{Q^{n+1} + U^{n-1}}{2}$ belongs to $\mathbb{K}^h$, equation (4.7) is verified and we set $U^{n+1} = Q^{n+1}$.
- If $\dfrac{Q^{n+1} + U^{n-1}}{2}$ is not in $\mathbb{K}^h$, we solve (4.7) with an augmented Lagrangian derived method, and set $U^{n+1} = 2\,\widetilde{U}^{n+1} - U^{n-1}$.

It has to be noticed that even if $\widetilde{U}^{n+1}$ belongs to $\mathbb{K}^h$, it doesn't mean that U^{n+1} belongs to $\mathbb{K}^h$. By the way, it doesn't but it is close. This phenomenon was also pointed out by Paoli–Schatzman [24].

Remark 4.2. The case of a singular mass matrix (Eq. (4.5)) is handled exactly in the same way as matrix $\frac{1}{\Delta t^2}\,\mathbf{M} + \beta\,\mathbf{K}$ has the same properties than the above defined matrix $\mathbf{A}$.

4.4. Numerical results for a clamped plate with Newmark type schemes for e = 0 or e = 1

A steel rectangular panel is considered, of width $L_1 = 40$ cm, length $L_2 = 120$ cm, and thickness $\varepsilon = 0.5$ cm. It means domain Ω is $]0, L_1[\times]0, L_2[$. The mechanical parameters are Young's modulus $E = 210$ GPa, Poisson's ratio $\nu = 0.3$ and mass density $\rho = 7.77\ 10^3$ kg/m^3. This plate is clamped along one edge and free along the three others. The numerical tests are performed with Getfem++ [13], using structured meshes (see Figs. 3 and 4).

Moreover, only the following kind of obstacle will be considered here (see (3.4) for definition of convex $\mathbb{K}^h$). It is a flat obstacle under the whole plate, which reads

$$g_2(x_1, x_2) = +\infty, \quad g_1(x_1, x_2) = -0.1, \quad \forall\ (x_1, x_2)\ \in\ \Omega. \tag{4.8}$$

Finally, as we are mainly interested to study conservation of energy, in all the next paragraphs, we consider the case where there is no loading $f(x,t) \equiv 0$ for all x and t. All energy is contained in an initial displacement u_0 , obtained as the static equilibrium of the plate under a constant load $f_0 = 14\,600$ N and an initial velocity $v_0 = 0$.

Remark 4.3. Other numerical tests are given in [28], such as flat symmetric obstacles along the plate and sine-sweep base forced vibration, with various frequencies. But, in that paper, only a e-β-Newmark scheme was used with only a regular mass matrix.

In this section, we only consider Newmark type schemes and we compare, on the one hand, the regular mass matrix discretization (4.1) with the singular one (4.5) and, on the other hand, the effect of the restitution coefficient e. Let us just observe that $e = 1$ is only tested with the singular mass matrix approach. So, the next figures give the numerical displacement of one corner of the plate, located on the edge opposite to the clamped one. For all Newmark schemes, parameter β is taken equal to $1/2$, which insures unconditional stability

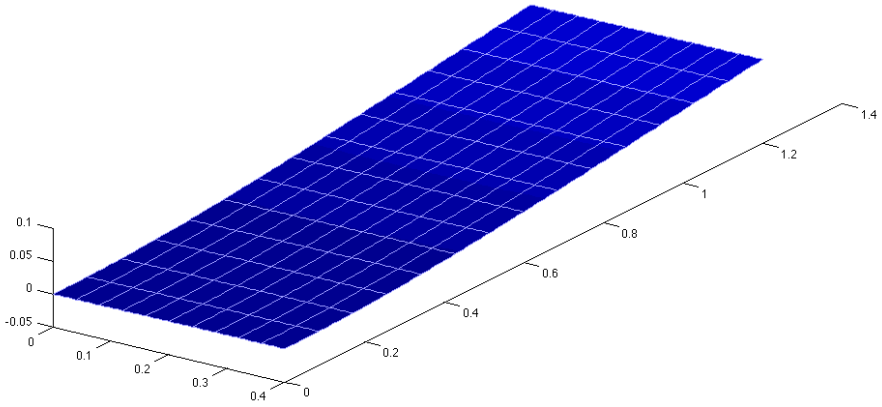

FIGURE 3. Bending clamped plate above a rigid obstacle: FVS quadrangular mesh.

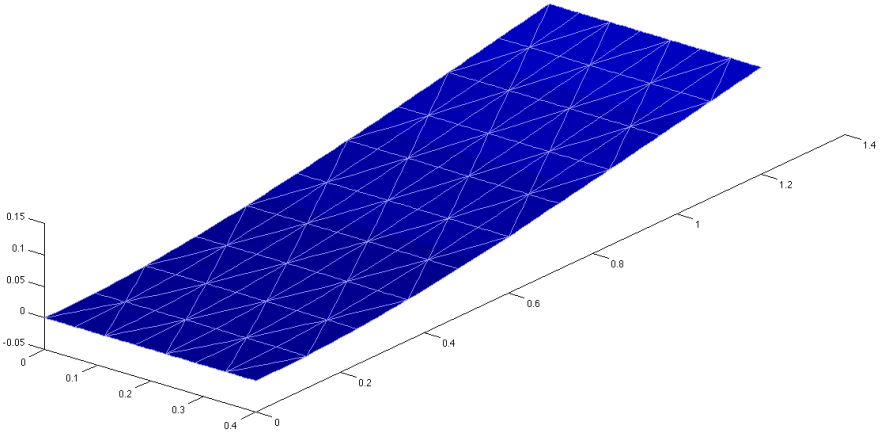

FIGURE 4. Bending clamped plate above a rigid obstacle: FVS quadrangular mesh.

when $e = 0$. Finally, complete and reduced HCT triangles, Argyris triangles and reduced FVS quadrangles are compared. As expected, it appears that displacements, which are obtained with $e = 1$, are less softened, at the beginning, than the others. However, these results are not obvious to interpret. So, we will focus on energy.

In the following computations, the effects on energy of the mass matrix discretization and of the restitution coefficient e are investigated. So, the discrete energy E_n reads

$$E_n = \frac{1}{8\Delta t^2}\,(U^{n+1} - U^{n-1})^T\,\mathbf{M}\,(U^{n+1} - U^{n-1}) + \frac{1}{2}\,(U^n)^T\,\mathbf{K}\,U^n,$$

as there is no loading.

Figures 9–11 give energy evolutions for different time steps, in the frame of a e-β-Newmark scheme, with $\beta = 1/2$.

First, let us observe the energy curves obtained for different time steps, with the singular mass matrix, when the restitution coefficient e is zero. Let us recall that the fully implicit scheme ($e = 0$) is known to be globally dissipative as illustrated for beams by numerical examples in [10]. Indeed, it can be seen the energy remains constant between two successive impacts and decreases only at these ones. Nevertheless, when the time step

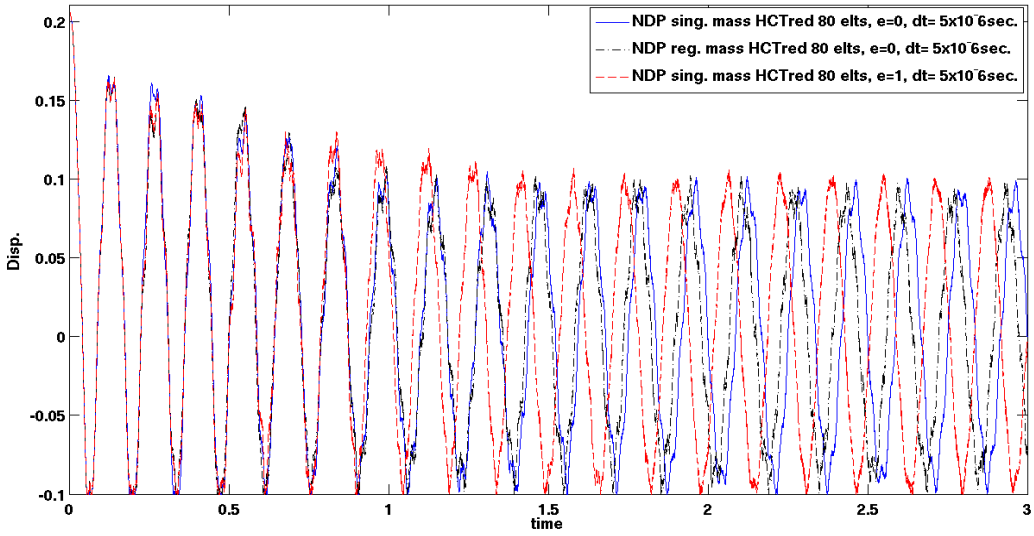

FIGURE 5. Reduced HCT, 80 triangles. e-β-Newmark scheme. $\Delta t = 5 \times 10^{-6}$. $e = 0$ or $e = 1$, regular or singular mass matrices.

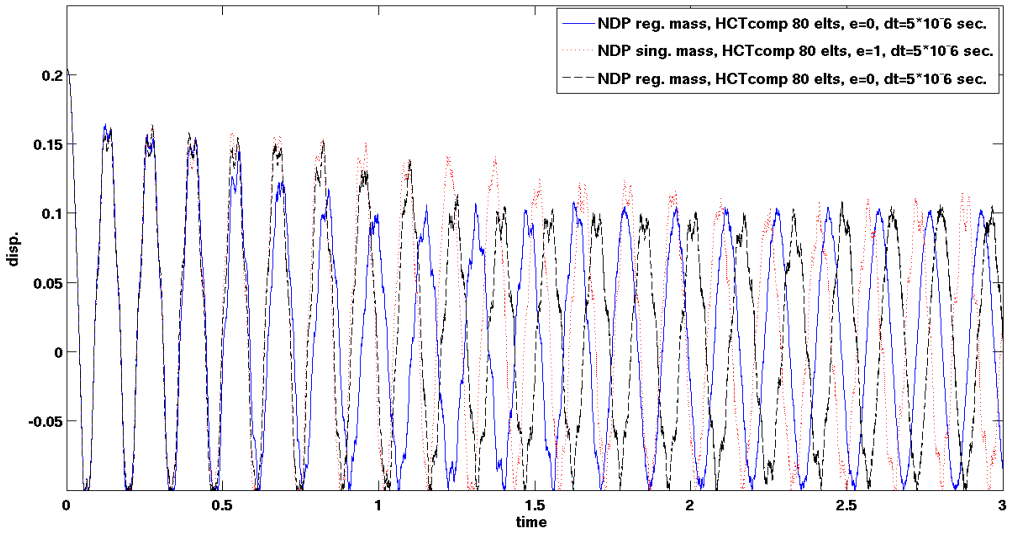

FIGURE 6. Complete HCT, 80 triangles. e-β-Newmark scheme. $\Delta t = 5 \times 10^{-6}$. $e = 0$ or $e = 1$, regular or singular mass matrices.

goes to zero, the loss of energy is weaker and weaker and it can be expected that energy conservation will hold at the limit. For comparison, the energy, obtained with regular mass matrix, is given only for the smallest time step. It appears that, with a singular mass matrix, the loss of energy is much lower than with a regular one.

Second, when $e = 1$, energy is weakly increasing but can be stabilized when the time step is sufficiently small. Moreover, it can be observed this condition seems more restrictive for triangles than for quadrangles, if it depends on the mesh size, as these ones are of the same order of magnitude in the case of our meshes (each quadrangle leads to two triangles, see Figs. 3 and 4).

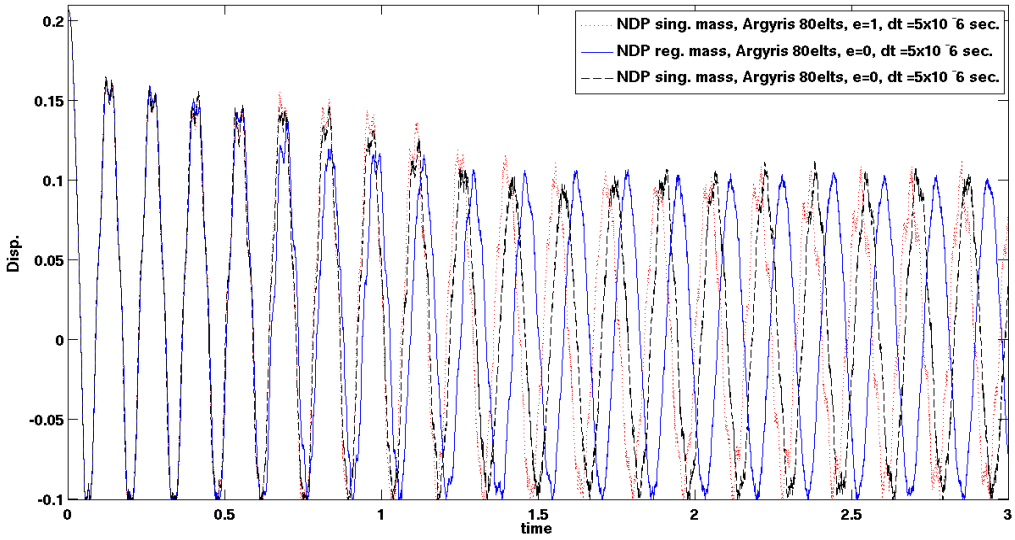

FIGURE 7. Argyris element, 80 triangles. e-β-Newmark scheme. $\Delta t = 5 \times 10^{-6}$. $e = 0$ or $e = 1$, regular or singular mass matrices.

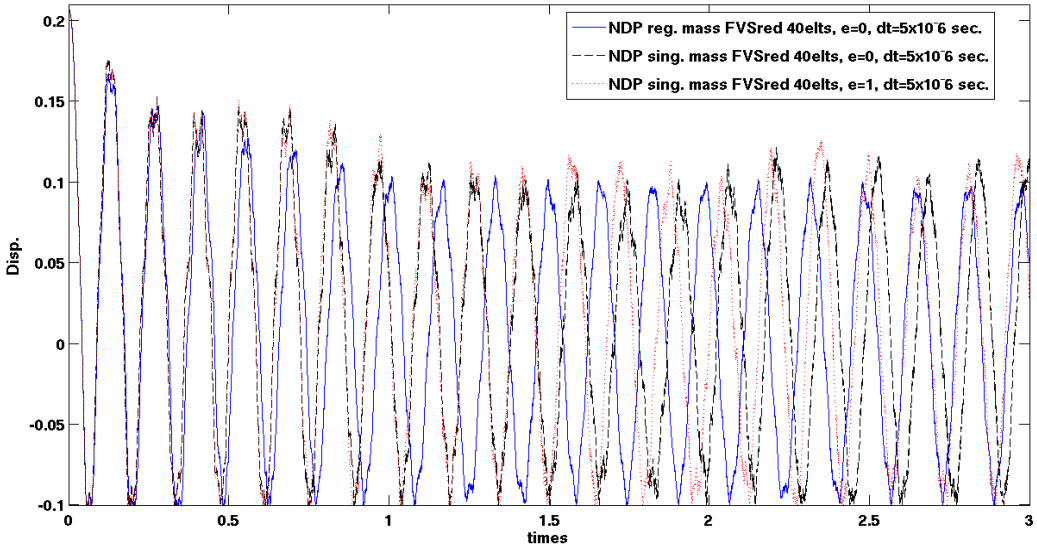

FIGURE 8. Reduced FVS, 40 quadrangles. e-β-Newmark scheme. $\Delta t = 5 \times 10^{-6}$. $e = 0$ or $e = 1$, regular or singular mass matrices.

Finally, it is worth to notice the effect of restitution coefficient e is hard to understand, in the case of the singular mass matrix. Indeed, if the numerical scheme is always dissipative when $e = 0$, and always energy increasing when $e = 1$, both seem to lead to an energy conserving scheme, when the time step goes to zero.

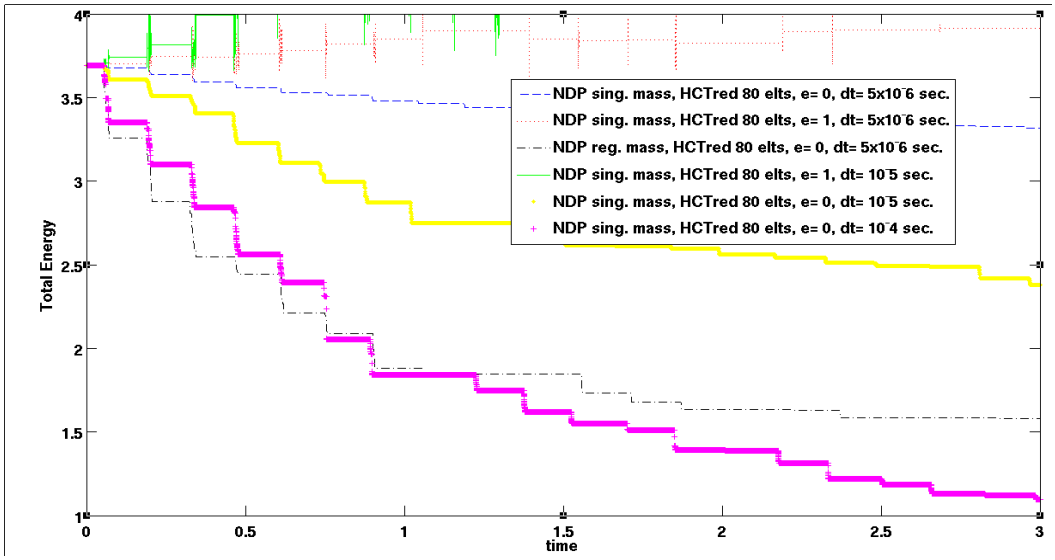

FIGURE 9. Energy for different time steps. Reduced HCT, 80 triangles. e-β-Newmark scheme. $e = 0$ or $e = 1$, regular or singular mass matrices.

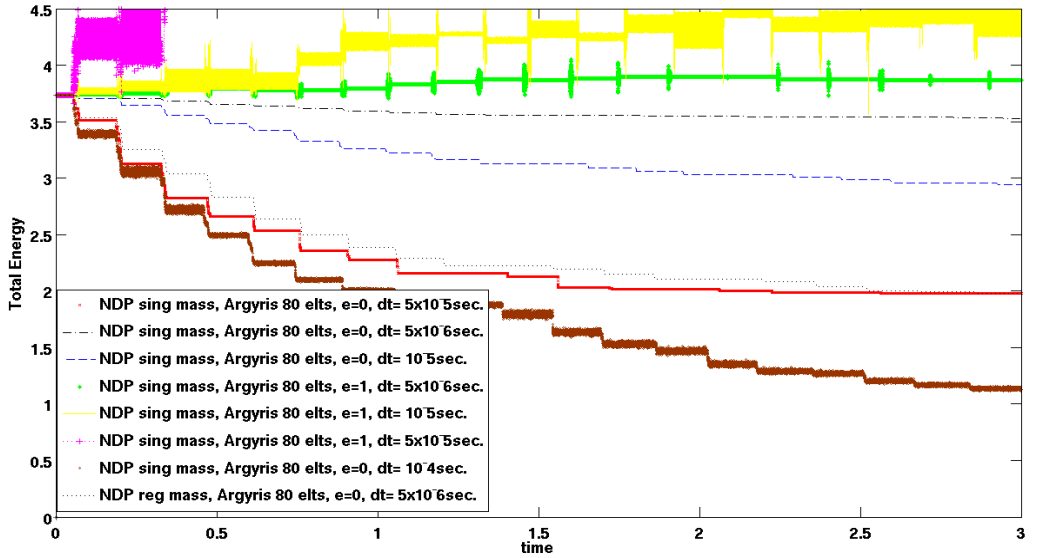

FIGURE 10. Energy for different time steps. Argyris element, 80 triangles. e-β-Newmark scheme. $e = 0$ or $e = 1$, regular or singular mass matrices.

4.5. Numerical results for a free plate with Newmark type schemes for $\mathbf{e = 0}$ or $\mathbf{e = 1}$

Now, the plate is free and all energy is contained in an initial velocity $v_0 = 1$ m/s, and the initial displacement $u_0 = 0$. There is still no loading $f(x,t) \equiv 0$ for all x and t. Moreover, there is only one impact in this case, during which the restitution coefficient e should play a crucial part.

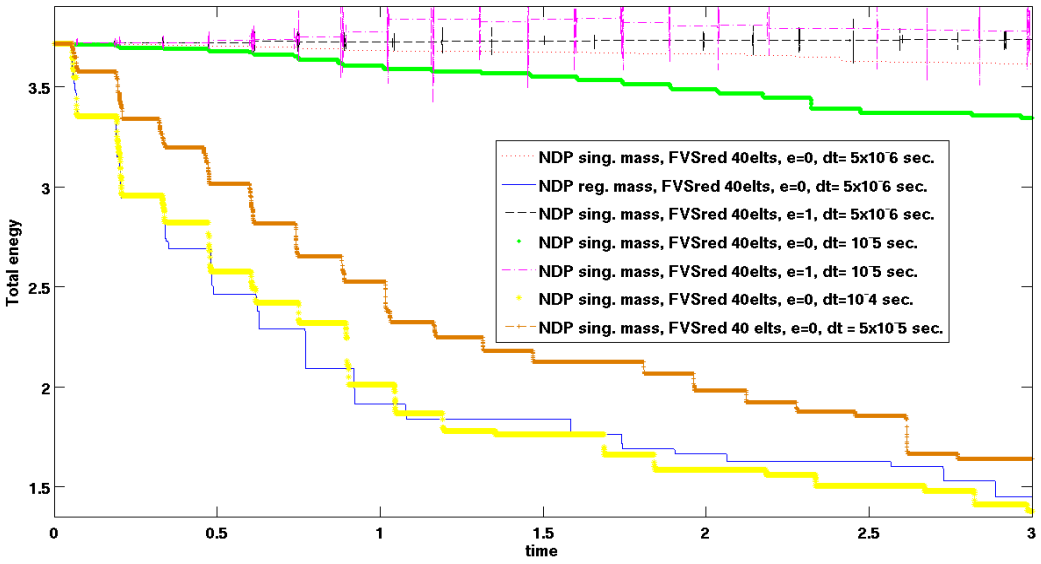

FIGURE 11. Energy for different time steps. Reduced FVS, 40 quadrangles. e-β-Newmark scheme. $e = 0$ or $e = 1$, regular or singular mass matrices.

First, as intended, let us observe that, in all cases, the energy is constant before and after impact. Then, as in the previous example, it can be seen that the fully implicit scheme ($e = 0$) remains dissipative while $e = 1$ leads to an energy increasing scheme, for both mass matrices. Nevertheless, these effects are weaker for the singular mass matrix than for the regular one. Moreover, as illustrated by displacement figures (Figs. 15–17), for our time step, the numerical solutions are very close for the singular mass matrix for both restitution coefficients. The question of the interpretation of this coefficient is again asked ourselves.

Finally, for both mass matrix schemes, it appears that the energy variation is the greatest for reduced HCT triangles and reduced FVS quadrangles, for which the magnitude is the same, and the lowest for Argyris triangles. Well, this last element is more precise than the previous ones, which have the same level of precision (see Sect. 3.1). This could explain the better numerical results we obtained in this case for Argyris element.

5. Fully discretized midpoint scheme

In this section, we recall and investigate midpoint scheme capabilities for time discretization, in the case of singular mass matrices. The goal of this section is then to show the performance of this scheme applied on the same benchmarks than in previous section.

5.1. Derivation of the midpoint scheme in the framework of a singular mass matrix

The midpoint scheme applied to problem (3.2) consists in finding $U^{n+1/2}$ in $\mathbb{K}^h$ such that (see for instance [29])

$$\begin{cases} (W - U^{n+1/2})^T \ (\mathbf{M}A^{n+1/2} + \mathbf{K}U^{n+1/2}) \ \geq \ (W - U^{n+1/2})^T \ F^n, \quad \forall W \in \mathbb{K}^h, \\ U^{n+1/2} = \dfrac{U^n + U^{n+1}}{2}, \quad V^{n+1/2} = \dfrac{V^n + V^{n+1}}{2}, \\ \mathbf{B}U^{n+1} = \mathbf{B}U^n + \Delta t \mathbf{C}V^{n+1/2}, \quad \mathbf{C}V^{n+1} = \mathbf{C}V^n + \Delta t \mathbf{B}A^{n+1/2}, \end{cases} \tag{5.1}$$

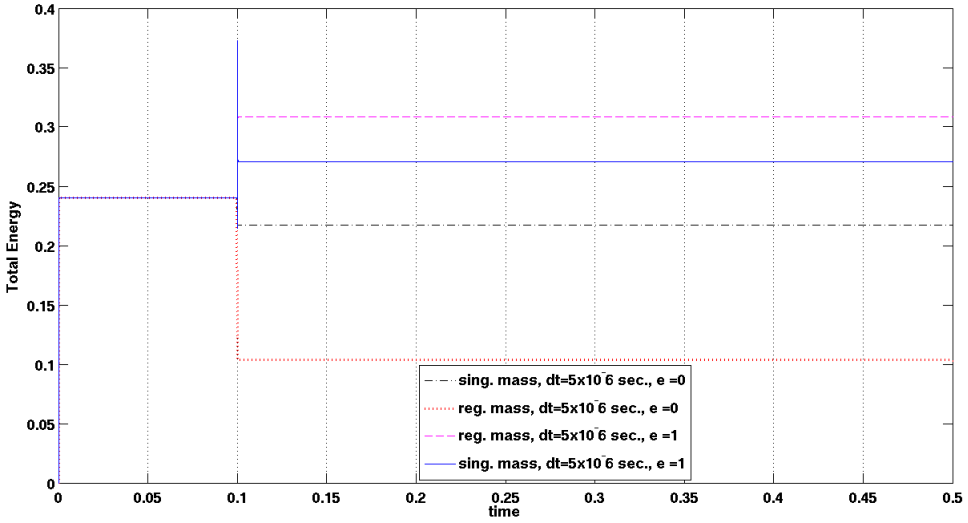

FIGURE 12. Energy evolution. Reduced HCT, 80 triangles. $\Delta t = 5 \times 10^{-6}$. e-β-Newmark scheme. $e = 0$ or $e = 1$, regular or singular mass matrices.

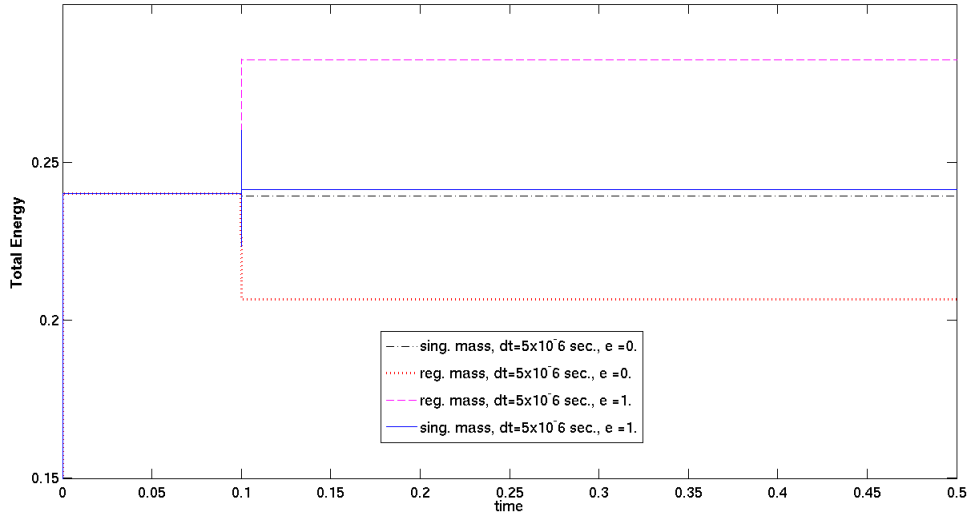

FIGURE 13. Energy evolution. Argyris element, 80 triangles. $\Delta t = 5 \times 10^{-6}$. e-β-Newmark scheme. $e = 0$ or $e = 1$, regular or singular mass matrices.

where $A^{n+1/2}$ is acceleration at "middle time step" $n + 1/2$. As matrix $\mathbf{C}$ is invertible, we have

$$V^{n+1} = 2V^{n+1/2} \; - \; V^n = 2\mathbf{C}^{-1}\,\mathbf{B}\,\frac{U^{n+1} - U^n}{\Delta t} \; - \; V^n = 4\mathbf{C}^{-1}\,\mathbf{B}\,\frac{U^{n+1/2} - U^n}{\Delta t} \; - \; V^n.$$

Moreover, $A^{n+1/2}$ can be eliminated in the following way

$$\mathbf{M}\,A^{n+1/2} = \mathbf{B}^T\,\mathbf{C}^{-1}\,\mathbf{B}\,A^{n+1/2} = \mathbf{B}^T\,\mathbf{C}^{-1}\,\frac{\mathbf{C}V^{n+1} - \mathbf{C}V^n}{\Delta t} = \mathbf{B}^T\,\frac{V^{n+1} - V^n}{\Delta t},$$

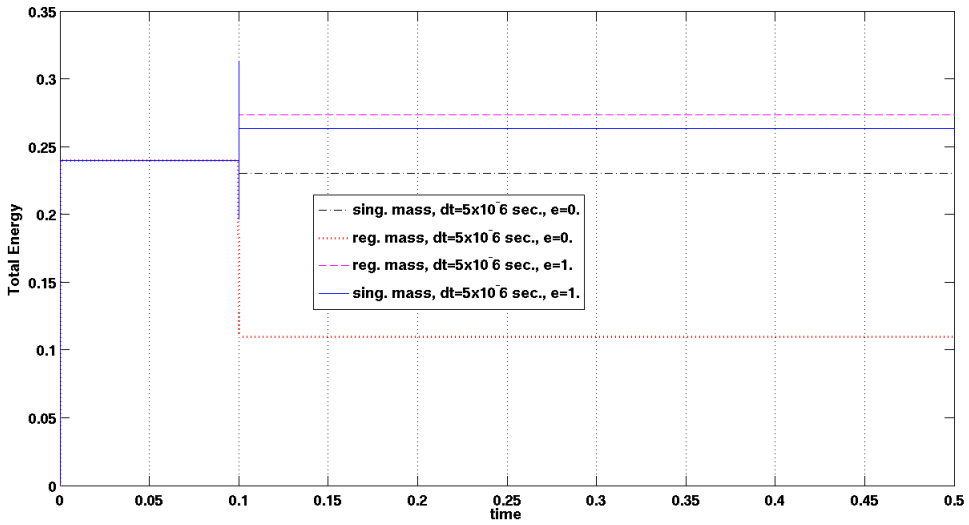

FIGURE 14. Energy evolution. Reduced FVS, 40 quadrangles. $\Delta t = 5 \times 10^{-6}$. e-β-Newmark scheme. $e = 0$ or $e = 1$, regular or singular mass matrices.

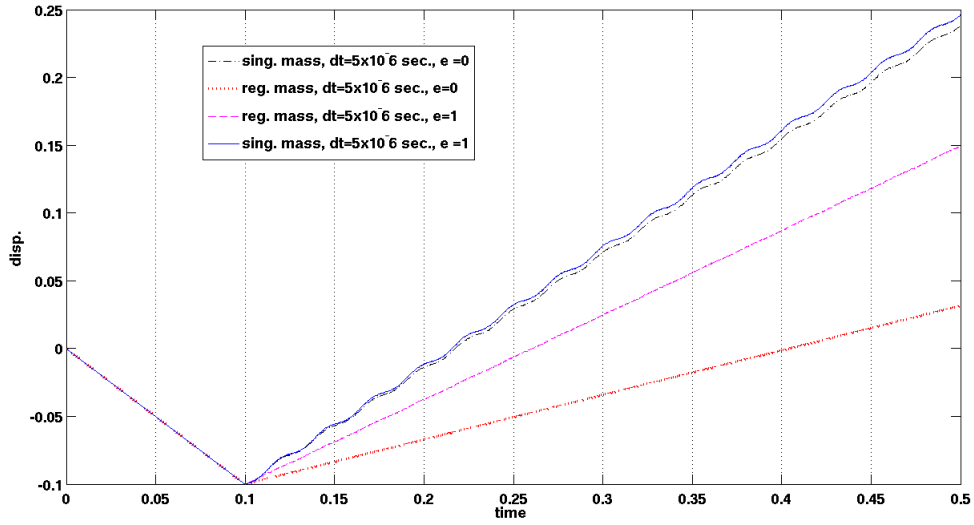

FIGURE 15. Displacement evolution. Reduced HCT, 80 triangles. $\Delta t = 5 \times 10^{-6}$. e-β-Newmark scheme. $e = 0$ or $e = 1$, regular or singular mass matrices.

or more explicitly

$$\mathbf{M}\ A^{n+1/2} = 4\mathbf{B}^T\ \mathbf{C}^{-1}\ \mathbf{B}\ \frac{U^{n+1/2} - U^n}{\Delta t^2} - 2\mathbf{B}^T\ \frac{V^n}{\Delta t} = \frac{4}{\Delta t^2}\mathbf{M}\ U^{n+1/2} - \frac{4}{\Delta t^2}\mathbf{M}\ U^n - \frac{2}{\Delta t}\mathbf{B}^T\ V^n.$$

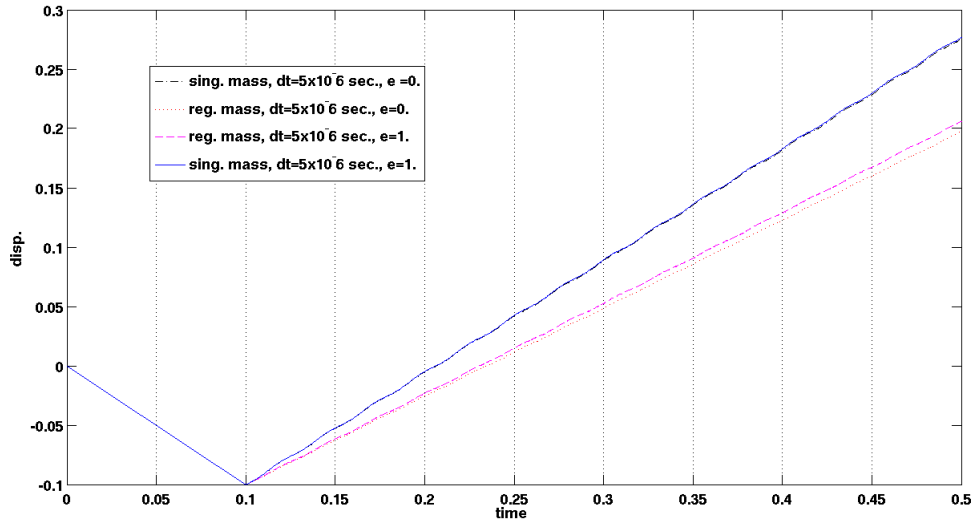

FIGURE 16. Displacement evolution. Argyris element, 80 triangles. $\Delta t = 5\times10^{-6}$. e-β-Newmark scheme. $e = 0$ or $e = 1$, regular or singular mass matrices.

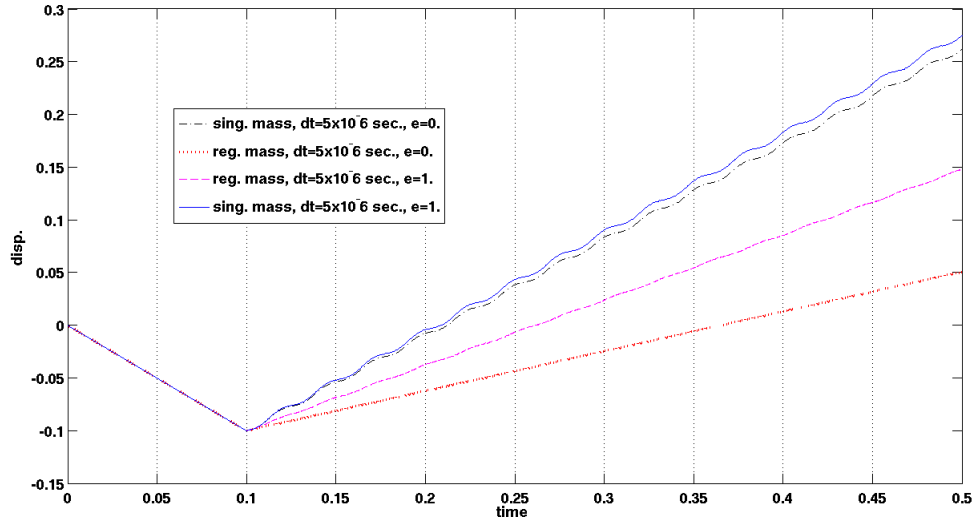

FIGURE 17. Displacement evolution. Reduced FVS, 40 quadrangles. $\Delta t = 5 \times 10^{-6}$. e-β-Newmark scheme. $e = 0$ or $e = 1$, regular or singular mass matrices.

Then, a new formulation of (5.1) is

$$\begin{cases} U^n \text{ and } V^n \text{ being given, find } U^{n+1/2} \in \mathbb{K}^h \text{ such that} \\ (W - U^{n+1/2})^T \left(\frac{4}{\Delta t^2}\mathbf{M}U^{n+1/2} + \mathbf{K}U^{n+1/2}\right) \geq (W - U^{n+1/2})^T \bar{F}^n, \quad \forall W \in \mathbb{K}^h, \\ \text{where } \bar{F}^n = F^n + \frac{4}{\Delta t^2}\mathbf{M}\, U^n + \frac{2}{\Delta t}\mathbf{B}^T\, V^n \\ U^{n+1} = 2U^{n+1/2} - U^n, \quad V^{n+1} = 2\mathbf{C}^{-1}\,\mathbf{B}\,\frac{U^{n+1}-U^n}{\Delta t} - V^n. \end{cases} \tag{5.2}$$

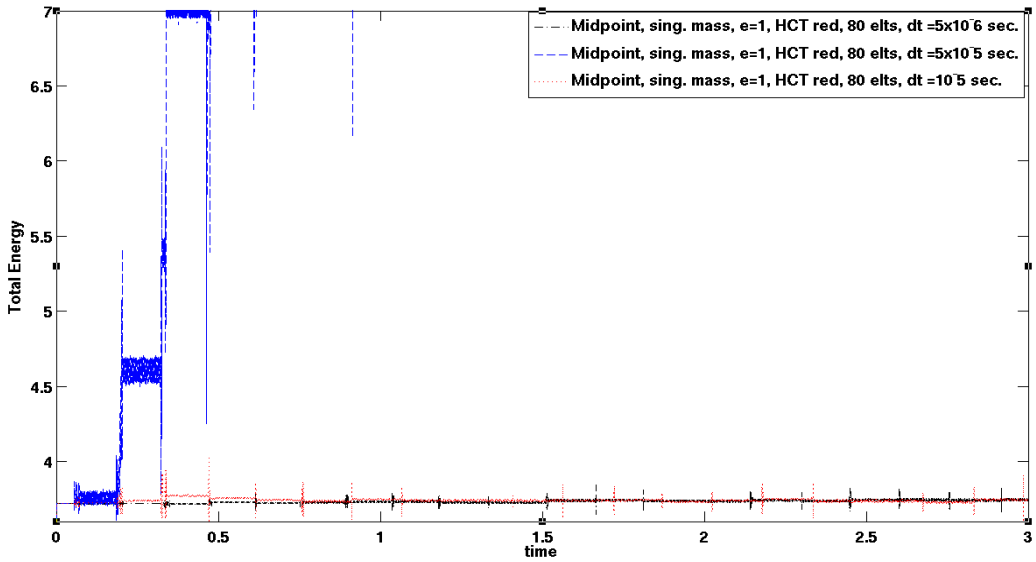

FIGURE 18. Energy for different time steps. Reduced HCT, 80 triangles. Midpoint scheme, singular mass matrix.

Exactly as for Newmark scheme, this variational inequality has always a unique solution even if $\mathbf{M}$ is singular.

Remark 5.1. The case $\mathbb{H}^h = \mathbb{V}^h$, which corresponds to the classical discretization where displacement and velocity are approximated in the same way, leads to a scheme similar to (5.2), the only differences being the singular mass matrix $\mathbf{M}$ is replaced by the regular one $\mathbf{M}_r$ and $\mathbf{C} = \mathbf{B} = \mathbf{B}^T$ so $\mathbf{C}^{-1}\,\mathbf{B} = I$. Finally, we do not prove the convergence of these schemes towards a solution of the continuous problem. Nevertheless, we shall observe good numerical results with singular mass discretization and instabilities for regular ones.

5.2. Numerical results for a clamped plate with midpoint scheme

In the following figures are given the energy evolutions for different time steps, for midpoint scheme with singular mass matrix. The regular mass matrix is not illustrated here as it is unstable. Moreover, this scheme involves no restitution coefficient e. So only the choice of finite elements can be addressed by these numerical results.

However, let us observe that midpoint scheme could correspond to a perfect elastic impact. Indeed, when a shock occurs, $U^{n+1/2}$ belongs to the boundary of $\mathbb{K}^h$. At this moment, "mechanically speaking", it means the corresponding velocity $V^{n+1/2}$ should be zero. Naturally, this condition is not prescribed in the numerical scheme, so is not true. Nevertheless, it is clear that $V^{n+1/2} = 0$ leads to $V^{n+1} = -V^n$: velocity just after impact is the same, up to its sign, than before. It is in that sense midpoint scheme would correspond to $e = 1$.

Keeping this remark in mind, we notice exactly the same phenomena than with e-β-Newmark scheme when $e = 1$. Energy is weakly increasing and can be stabilized when the time step decreases. And the numerically observed stability condition seems to be more restrictive for triangles than for quadrangles.

5.3. Numerical results for a free plate with midpoint scheme

Now, the plate is free and all energy is contained in an initial velocity $v_0 = 1$ m/s, the initial displacement being $u_0 = 0$. There is still no loading $f(x,t) \equiv 0$ for all x and t.

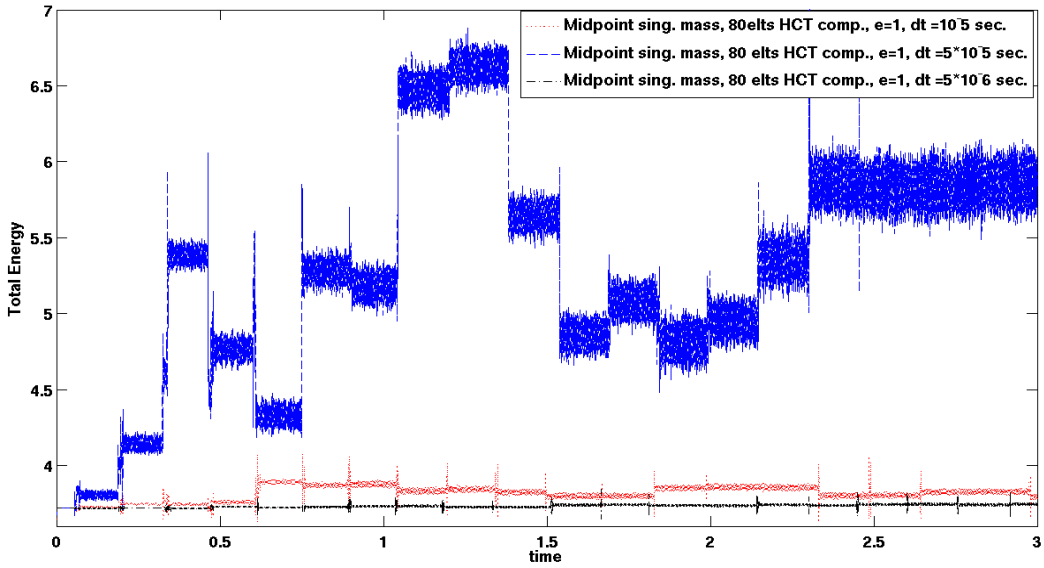

FIGURE 19. Energy for different time steps. Complete HCT, 80 triangles. Midpoint scheme, singular mass matrix.

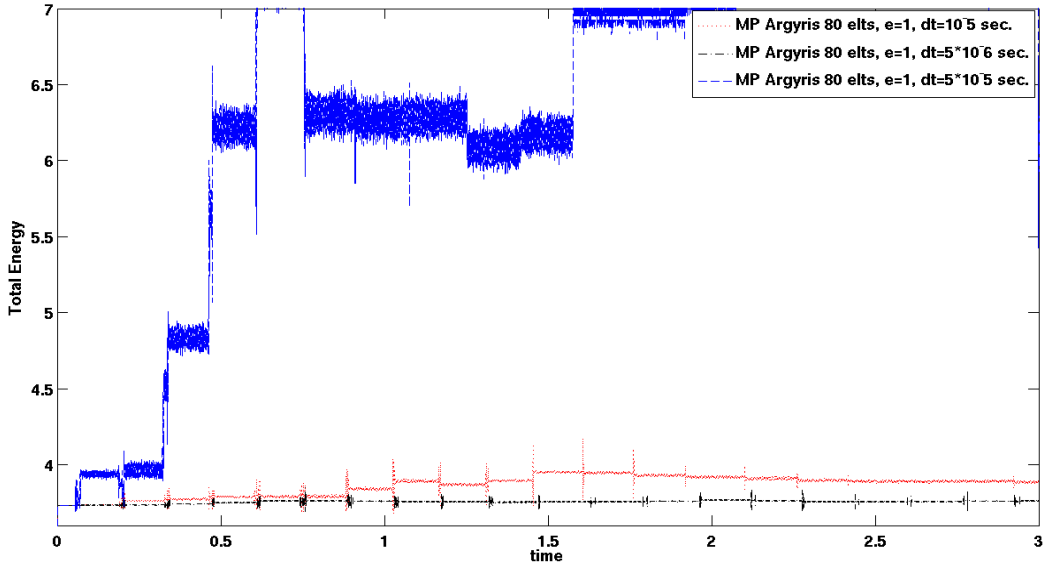

FIGURE 20. Energy for different time steps. Argyris element, 80 triangles. Midpoint scheme, singular mass matrix.

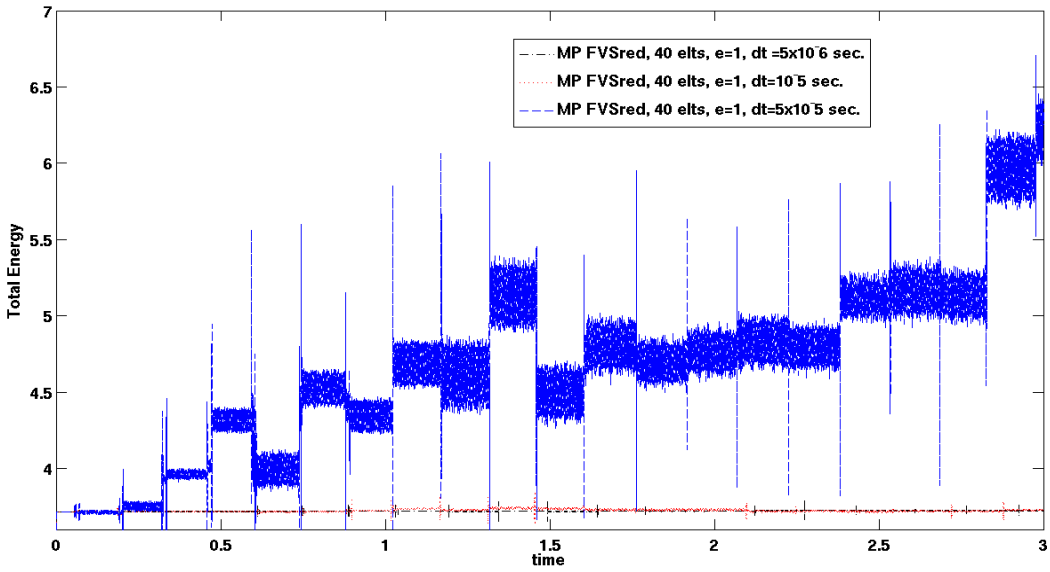

FIGURE 21. Energy for different time steps. Reduced FVS, 40 quadrangles. Midpoint scheme, singular mass matrix.

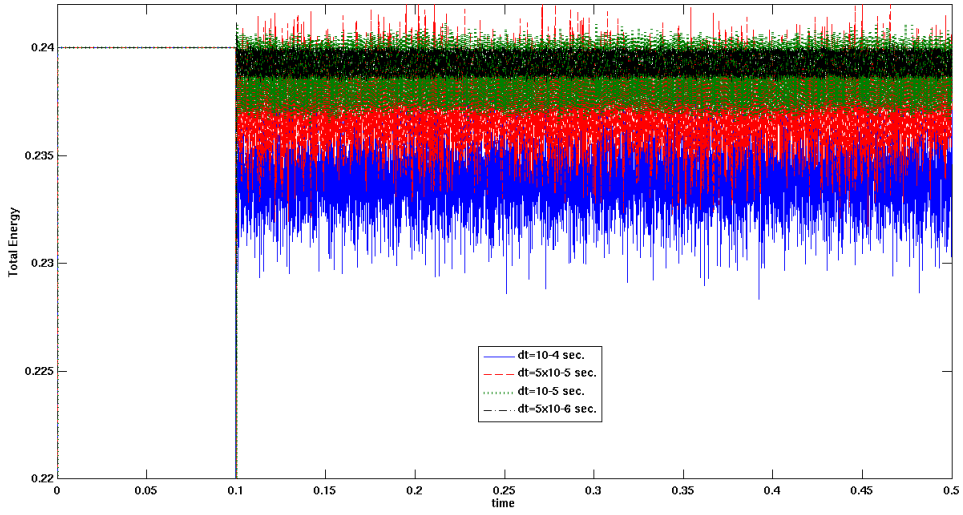

FIGURE 22. Energy for different time steps. Reduced HCT, 80 triangles. Midpoint scheme with singular mass matrix.

Figures 22–24 give energy evolutions for different time steps, for midpoint scheme with singular mass matrix. It can be noticed that energy is weakly increasing and can be stabilized when the time step decreases. Moreover, the numerically observed stability condition seems to be more restrictive for triangles than for quadrangles.

Finally, displacements of free corners are given Figures 25–27. It appears the curves are the closest in the case of Argyris element, while they are very similar for reduced HCT and reduced FVS. Like Newmark scheme, it could originate in the precision of these elements.

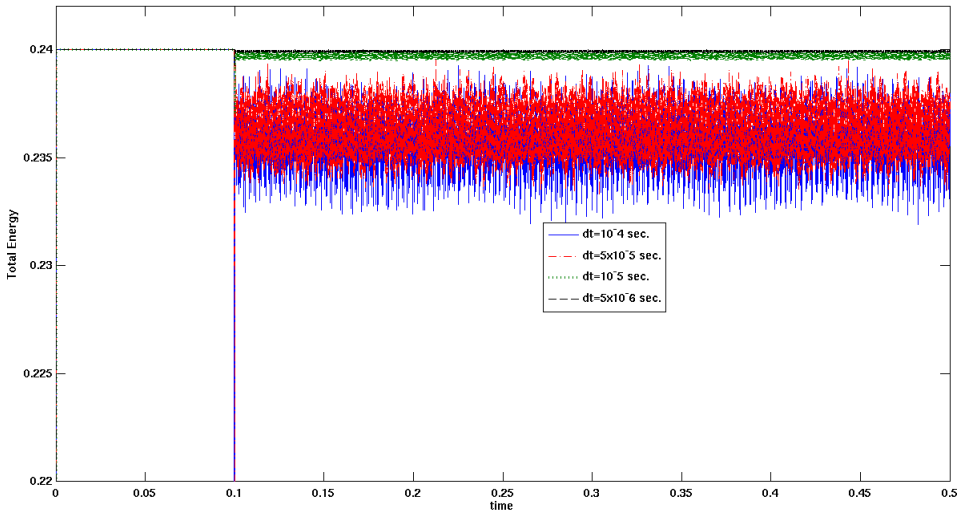

FIGURE 23. Energy for different time steps. Argyris element, 80 triangles. Midpoint scheme with singular mass matrix.

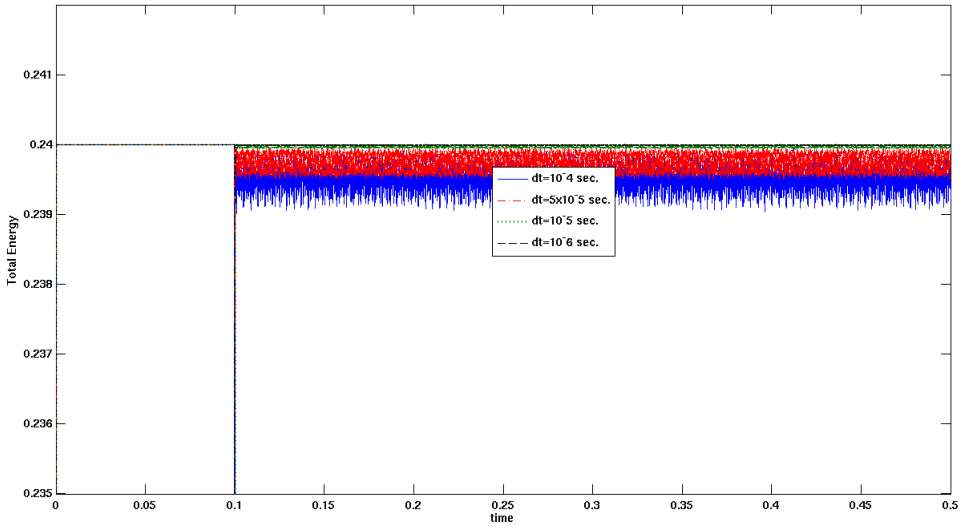

FIGURE 24. Energy for different time steps. Reduced FVS, 40 quadrangles. Midpoint scheme with singular mass matrix.

5.4. Semi-analytical solution for free impact of a rectangular panel

Now, we would like to summarize a brief analysis of the previous free impact problem which corresponds to a loading $f(x,t) = 0$ (except when impact occurs), initial position $u_0(x) = 0$ and initial velocity $v_0(x) = -1$, the obstacle being flat at level $g_1(x) = -0.1$, for all $x \in \Omega$.

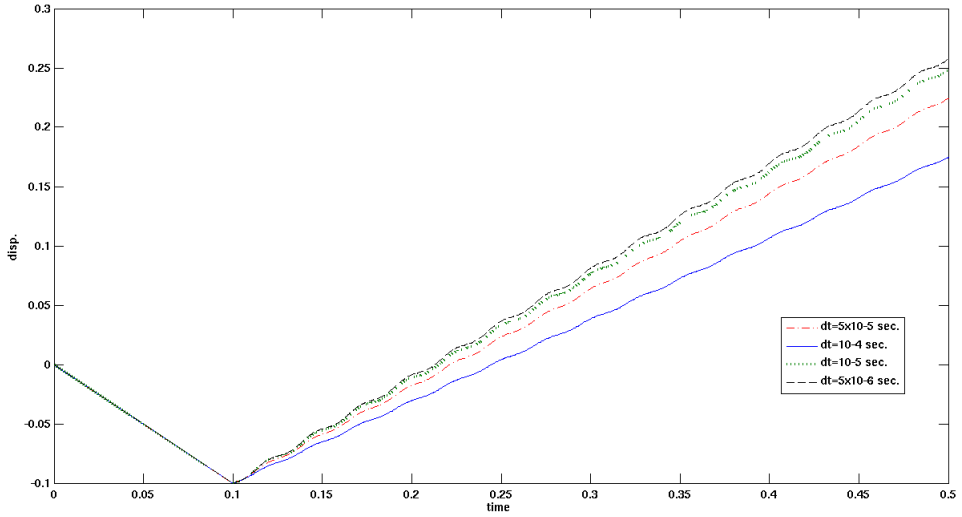

FIGURE 25. Displacement for different time steps. Reduced HCT, 80 triangles. Midpoint scheme with singular mass matrix.

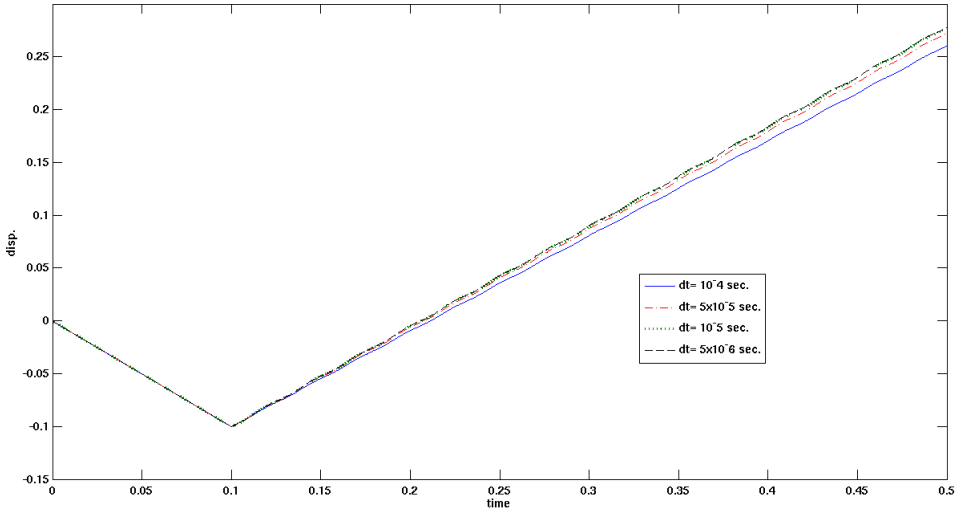

FIGURE 26. Displacement for different time steps. Argyris element, 80 triangles. Midpoint scheme with singular mass matrix.

First, let us observe that, if the plate is considered as a rigid body, the exact solution of our impact problem is a rigid body vertical translation, which reads

$$\tilde{u}_1(t) = |v_0(t - t_{\text{impact}})| + g_1.$$

for a perfect impact ($e = 1$), while the totally dissipative solution, corresponding to $e = 0$, is

$$\tilde{u}_0(t) = [v_0\ (t - t_{\text{impact}}) + g_1]\ \mathbb{1}_{]0,t_{\text{impact}}[}(t),$$

$\mathbb{1}_{]0,t_{\text{impact}}[}$ being the indicatrice function for interval $]0, t_{\text{impact}}[$. It can be noted that the previous numerical experiments confirm such a behavior before impact, for all numerical schemes, with all mass matrices.

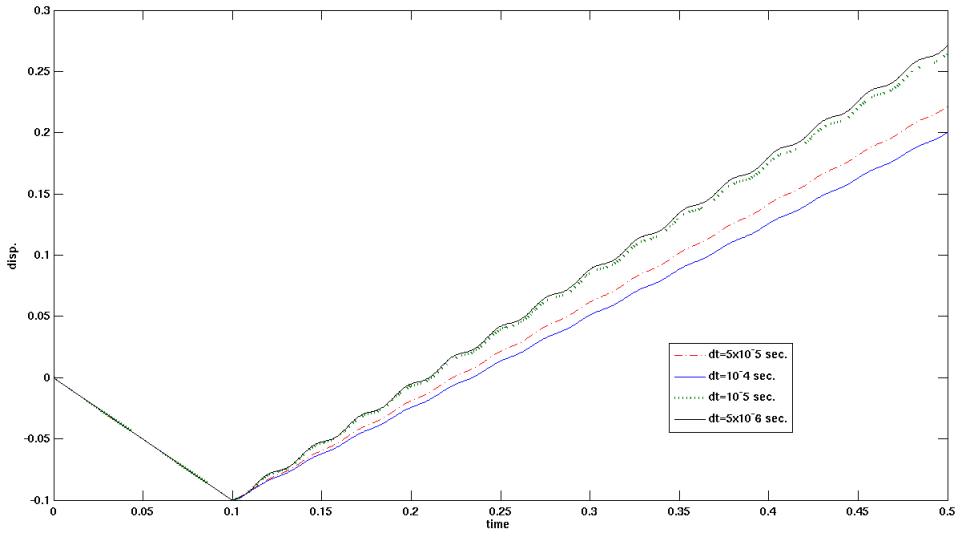

FIGURE 27. Displacement for different time steps. Reduced FVS, 40 quadrangles. Midpoint scheme with singular mass matrix.

Now, let us consider the plate as an elastic body. Then, we set $\Gamma_c = \emptyset$ in (2.4), and we assume the plate is rectangular: $\Omega =]0, L_1[\times]0, L_2[$. Under these assumptions, we rewrite (2.8) as a single impact problem at t_{impact}, and displacement u verifies in the distributions sense the equation

$$2\rho\varepsilon\ddot{u} + K(u) = 2\rho\varepsilon\ e\ \delta_{t=t_{\text{impact}}} \quad \text{with} \quad u \in \mathbb{K} \quad \text{and} \quad K = \frac{2E\ \varepsilon^3}{3\ (1-\nu^2)}\ \Delta^2. \tag{5.3}$$

Since the fourth order differential operator K is an elliptic self-adjoint operator, with our boundary conditions, there exists a sequence of real eigenvalues $0 = \lambda_0 \leq \lambda_1 \leq \lambda_2 \leq \ldots \leq \lambda_i \leq \ldots$, with $\lim_i \lambda_i = \infty$. Moreover, the eigenfunctions φ_i are an orthonormal basis of $\mathbb{H}$ in the sense of the mass operator, that means

$$\int_\Omega 2\rho\varepsilon\ \varphi_i(x)\ \varphi_j(x)\ \mathrm{d}x = \delta_{ij}$$

where δ_{ij} is the Kronecker symbol, and φ_i satisfy

$$\begin{cases} K(\varphi_i) = \lambda_i \varphi_i \quad \text{on} \quad \Omega \\ \\ \text{Boundary conditions on} \quad \partial\Omega \end{cases} \tag{5.4}$$

with $\varphi_i(x_1, x_2) = \varphi_{2i-1}(x_1)\ \varphi_{2i}(x_2)$ and

$$\begin{cases} \varphi_{2i-1}(x_1) = A_{2i-1}\cosh(\lambda_{2i-1}^{\frac{1}{4}}(x_1)) + B_{2i-1}\cos(\lambda_{2i-1}^{\frac{1}{4}}x_1) + C_{2i-1}\sinh(\lambda_{2i-1}^{\frac{1}{4}}x_1) + D_{2i-1}\sin(\lambda_{2i-1}^{\frac{1}{4}}x_1), \\ \varphi_{2i}(x_2) \quad = A_{2i}\cosh(\lambda_{2i}^{\frac{1}{4}}x_2) + B_{2i}\cos(\lambda_{2i}^{\frac{1}{4}}x_2) + C_{2i}\sinh(\lambda_{2i}^{\frac{1}{4}}x_2) + D_{2i}\sin(\lambda_{2i}^{\frac{1}{4}}x_2). \end{cases}$$

With the boundary conditions, we have a homogeneous system to determine A_i, B_i, C_i, D_i and λ_i. Unfortunately, there is no exact analytical solution φ_i for a rectangular plate free on four edges. Exact solutions to the vibration of rectangular plates are only available for plates with two opposite edges subject to simply supported or clamped conditions. Otherwise, they are analysed by using approximate methods [31]. Nevertheless, it is possible to obtain a very good approximation of the eigenvalues and eigenvectors associated to a free rectangular

plate, and express the displacement u solution of (5.3) in semi-analytical form. Then we can write

$$u(x,t) = \sum_{i\geq 1} q_i(t)\ \varphi_i(x).$$

Introducing this expression in the more general form of (5.3), which can be written

$$\ddot{u} + K(u) = f(x,t) \quad \text{on} \quad \Omega\times]0,T[,$$

we obtain

$$f = \sum_{i\geq 1} \ddot{q}_i(t)\ \varphi_i(x) + \sum_{i\geq 1} q_i(t)\ K(\varphi_i)(x) = \sum_{i\geq 1} \ddot{q}_i(t)\ \varphi_i(x) + \sum_{i\geq 1} \lambda_i\ q_i(t)\ \varphi_i(x)$$

which leads to

$$\ddot{q}_i(t) + \lambda_i\ q_i(t) = f_i(t)\ \equiv\ \int_\Omega 2\rho\varepsilon\ \varphi_i(x)\ f(x,t)\ \mathrm{d}x,$$

associated with the initial conditions

$$u(x,0) = \sum_{i\geq 1} q_i(0)\ \varphi_i(x) = 0 \quad \Rightarrow \quad q_i(0) = 0,$$

and

$$\dot{u}(x,0) = \sum_{i\geq 1} \dot{q}_i(0)\ \varphi_i(x) = v_0 \quad \Rightarrow \quad \dot{q}_i(0) = v_{0i}\ \equiv\ \int_\Omega 2\rho\varepsilon\ \varphi_i(x)\ v_0(x)\ \mathrm{d}x.$$

So, in our case, before impact, where $f(x,t) = 0$ and $v_0 = -1$, we obtain

$$q_i(t) = \frac{v_{0i}}{\sqrt{\lambda_i}}\ \sin(\sqrt{\lambda_i}\ t) = -2\rho\varepsilon\ \frac{\displaystyle\int_\Omega \varphi_i(x)\ \mathrm{d}x}{\sqrt{\lambda_i}}\ \sin(\sqrt{\lambda_i}\ t).$$

However, this part of the analytical solution can be omitted as the plate acts as a rigid body.

At impact, occuring at t_{impact}, we have $u(x,t_{\text{impact}}) = g_1$ and $\dot{u}(x,t_{\text{impact}}) = -e\ v_0$ (if we assume a rigid body behavior of the plate). The problem to be solved reads

$$\ddot{u} + K(u) = f(x,t) = 0 \quad \text{on} \quad \Omega\times]t_{\text{impact}},T[,$$

associated with the previous initial conditions. This problem can be solved as before and we have

$$q_i(t) = q_i(t_{\text{impact}})\ \cos(\sqrt{\lambda_i}\ (t - t_{\text{impact}})) + \dot{q}_i(t_{\text{impact}})\ \frac{\sin(\sqrt{\lambda_i}\ (t - t_{\text{impact}}))}{\sqrt{\lambda_i}},$$

with

$$\begin{cases} q_i(t_{\text{impact}}) = \displaystyle\int_\Omega 2\rho\varepsilon\ \varphi_i(x)\ g_1\ \mathrm{d}x = 2\rho\varepsilon\ g_1\ \int_\Omega \varphi_i(x)\ \mathrm{d}x, \\ \dot{q}_i(t_{\text{impact}}) = \displaystyle\int_\Omega 2\rho\varepsilon\ \varphi_i(x)\ (-e\ v_0)\ \mathrm{d}x = -2\rho\varepsilon\ e\ v_0\ \int_\Omega \varphi_i(x)\ \mathrm{d}x. \end{cases}$$

Impact excites linear modes of the plate, which are the eigenfunctions of operator K. Then the solution presents free vibrations as we can see on the previous numerical tests. Finally, the singular dynamic method tends to select the conservative solution of (5.3). Thank to this remarks, numerical convergence between semi-analytical and numerical solutions to compare the properties of standard and reduced mass approaches has to be investigated in future works.

6. Conclusion

This paper presents an application of the Singular Dynamic Method to fourth order plate impact problems. This strategy has proved its capabilities as illustrated by numerous numerical results. Two schemes, which are conservative in energy, are disclosed. The following of this work would be to improve this model by taking into account friction and damping. On a more theoretical point of view, strong convergence of the discrete solution has also to be adressed. Let us just discuss some points very briefly. Ahn and Stewart [2] show that the amount of energy in high frequency modes, related to the fourth-order operator, is almost zero under the assumption of strong convergence to the solution of the elastodynamic problem for a beam between rigid obstacles. From a mechanical point of view, it means that high frequency modes would be damped. As the singular mass matrix method transforms the elastodynamic inequality problem (2.8) into a Lipschitz-O.D.E., for a given space step, every convergent scheme for a Lipschitz-O.D.E. will converge when Δt goes to zero, and the limit is obviously the unique solution of (3.2) which is conservative. So, if it can be proved the weak convergence of the solution of (4.5) to the problem (2.8), the strong convergence will follow from the balance of energy with the singular mass matrix (3.3). However, a new problem occurs. Indeed, equation (2.8) doesn't include the restitution coefficient introduced by (2.9), nor the derived Lipschitz-O.D.E. Consequently, the complete link between fully discretized schemes, including restitution coefficient, and initial P.D.E. has to be investigated in depth. In particular, the main difficulty is to write the continuous problem associated to a singular mass operator and, also, to take into account that velocity is a bounded variation function, including its reliance on restitution coefficient.

References

[1] R.A. Adams, *Sobolev spaces*. Academic Press (1975).

[2] J. Ahn and D.E. Stewart, An Euler-Bernoulli beam with dynamic contact: Discretization, convergence and numerical results. *SIAM J. Numer. Anal.* **43** (2005) 1455–1480.

[3] P. Alart and A. Curnier, A mixed formulation for frictional contact problems prone to Newton like solution methods. *Comput. Methods Appl. Mech. Eng.* **92** (1991) 353–375.

[4] B. Brogliato, *Nonsmooth Mechanics*, edited by E.D. Sontag, M. Thoma. Springer, London (1999).

[5] N.J. Carpenter, Lagrange constraints for transient finite element surface contact. *Int. J. Numer. Methods Eng.* **32** (1991) 103–128.

[6] P.G. Ciarlet, *The finite element method for elliptic problems*. North-Holland (1978).

[7] P.G. Ciarlet, Basic error estimates for elliptic problems, in Vol. II of *Handbook of Numerical Analysis*. North-Holland (1991) 17–351.

[8] F. Dabaghi, A. Petrov, J. Pousin and Y. Renard, Convergence of mass redistribution method for the wave equation with a unilateral constraint at the boundary *ESAIM: M2AN* **48** (2014) 1147–1169.

[9] P. Deuflhard, R. Krause and S. Ertel, A contact-stabilized Newmark method for dynamical contact problems. *Int. J. Numer. Methods Eng.* **73** (2007) 1274–1290.

[10] Y. Dumont and L. Paoli, Vibrations of a beam between obstacles: Convergence of a fully discretized approximation. *ESAIM: M2AN* **40** (2006) 705–734.

[11] Y. Dumont and L. Paoli, Numerical simulation of a model of vibrations with joint clearance. *Int. J. Comput. Appl. Technol.* **33** (2008) 41–53.

[12] D. Doyen, *Méthodes numériques pour des problèmes dynamiques de contact et de fissuration*. Thèse de l'Université Paris-Est (2010).

[13] Y. Renard and J. Pommier, An open source generic C++ library for finite element methods. Available at http://home.gna.org/getfem/ (2016).

[14] C. Hager, S. Hüeber and B. Wohlmuth, A stable energy conserving approach for frictional contact problems based on quadrature formulas. *Int. J. Numer. Methods Eng.* **73** (2008) 205–225.

[15] P. Hauret and P. Le Tallec, Energy controlling time integration methods for nonlinear elastodynamics and low-velocity impact. *Comput. Methods Appl. Mech. Eng.* **195** (2006) 4890–4916.

[16] P. Hauret, Mixed Interpretation and Extensions of the Equivalent Mass Matrix Approach for Elastodynamics with Contact. *Comput. Methods Appl. Mech. Eng.* **199** (2010) 2941–2957.

[17] R.A. Ibrahim, V.I. Babitsky and M. Okuma, Vibro-Impact Dynamics of Ocean Systems and Related Problems. Vol. 44 of *Lect. Notes Appl. Comput. Mech.* Springer (2009).

[18] H.B. Khenous, P. Laborde and Y. Renard, Mass redistribution method for finite element contact problems in elastodynamics. *Eur. J. Mech., A/Solids* **27** (2008) 918–932.

[19] K. Kuttler and M. Shillor, Vibrations of a beam between two stops, Dynamics of Continuous, Discrete and Impulsive Systems. *Ser. B, Appl. Algorithms* **8** (2001) 93–110.

[20] T.A. Laursen and V. Chawla, Design of energy conserving algorithms for frictionless dynamic contact problems. *Int. J. Numer. Methods Eng.* **40** (1997) 863–886.

[21] T.A. Laursen and G.R. Love, Improved implicit integrators for transient impact problems-geometric admissibility within the conserving framework. *Int. J. Numer. Methods Eng.* **53** (2002) 245–274.

[22] L. Paoli, Time discretization of vibro-impact. *Philos. Trans. R. Soc. Lond.*, A **359** (2001) 2405–2428.

[23] L. Paoli and M. Schatzman, A numerical scheme for impact problems. I. The one-dimensional case. *SIAM J. Numer. Anal.* **40** (2002) 702–733.

[24] L. Paoli and M. Schatzman, Numerical simulation of the dynamics of an impacting bar. *Comput. Methods Appl. Mech. Eng.* **196** (2007) 2839–2851.

[25] A. Petrov and M. Schatzman, Viscoélastodynamique monodimensionnelle avec conditions de Signorini. *C. R. Acad. Sci. Paris*, I **334** (2002) 983–988.

[26] A. Petrov and M. Schatzman, A pseudodifferential linear complementarity problem related to a one dimensional viscoelastic model with Signorini condition. *Archive for Rational Mechanics and Analysis*. Springer (2009).

[27] C. Pozzolini and M. Salaün, Some energy conservative schemes for vibro-impacts of a beam on rigid obstacles. *ESAIM: M2AN* **45** (2011) 1163–1192.

[28] C. Pozzolini, Y. Renard and M. Salaün, Vibro-Impact of a plate on rigid obstacles: existence theorem, convergence of a scheme and numerical simulations. *IMA J. Numer. Anal.* **33** (2013) 261–294.

[29] Y. Renard, The singular dynamic method for constrained second order hyperbolic equations. Application to dynamic contact problems. *J. Comput. Appl. Math.* **234** (2010) 906–923.

[30] R.L. Taylor and P. Papadopoulos, On a finite element method for dynamic contact-impact problems. *Int. J. Numer. Methods Eng.* **36** (1993) 2123–2140.

[31] Y. Mochida, *Bounded Eigenvalues of Fully Clamped and Completely Free Rectangular Plates.* Master thesis of the University of Waikato Hamilton, New Zealand (2007).